8-3-2007

A Mechanism of Co-Existence of Bursting and Silent Regimes of Activities of a Neuron

Tatiana Igorevna Malashchenko

A MECHANISM OF CO-EXISTENCE OF BURSTING AND SILENT REGIMES OF ACTIVITIES OF A NEURON

by

TATIANA MALASCHENKO

Under the direction of Gennady S. Cymbalyuk

and

the co-direction of Andrey Shilnikov

ABSTRACT

The co-existence of bursting activity and silence is a common property of various neuronal models. We describe a *novel* mechanism explaining the co-existence of and the transition between these two regimes. It is based on the specific homoclinic and Andronov-Hopf bifurcations of the hyper- and depolarized steady states that determine the co-existence domain in the parameter space of the leech heart interneuron models: canonical and simplified. We found that a sub-critical Andronov-Hopf bifurcation of the hyperpolarized steady state gives rise to small amplitude sub-threshold oscillations terminating through the secondary homoclinic bifurcation. Near the corresponding boundary the system can exhibit long transition from bursting oscillations into silence, as well as the bi-stability where the observed regime is determined by the initial state of the neuron. The mechanism found is shown to be generic for the simplified 4D and the original 14D leech heart interneuron models.

INDEX WORDS: Bursting, silence, co-existence, multistability, bifurcation analysis, computational neuroscience, Master of Science, Georgia State University

A MECHANISM OF CO-EXISTENCE OF BURSTING AND SILENT REGIMES OF ACTIVITIES OF A NEURON

by

TATIANA MALASCHENKO

Thesis Submitted in Partial Fulfillment of the Requirements for the Degree of

Master of Science

in the College of Arts and Sciences

Georgia State University

2007

A MECHANISM OF CO-EXISTENCE OF BURSTING AND SILENT REGIMES OF ACTIVITIES OF A NEURON

by

TATIANA IGOREVNA MALASCHENKO

Major Professor: Gennady Cymbalyuk

Committee: Andrey Shilnikov

Donald Edwards

Vadym Apalkov

Unil Perera

Electronic Version Approved:

Office of Graduate Studies

College of Arts and Sciences

Georgia State University

August 2007

TABLE OF CONTENTS

LIST OF TABLES v

LIST OF FIGURES v

LIST OF DIAGRAMS vi

CHAPTER

1 INTRODUCTION 1

Types of neuron activities 1

Advantages of studying cellular mechanisms of neuronal dynamics in invertebrates 2

Bifurcations in the model and the transitions between different types of electrical activities 5

2 METHODS 8

3 RESULTS 12

Simplified model 12

Window current mode of I_{Na} 13

Canonical parameters of model (I_{CaS}, I_{Na}) 14

Bifurcation analysis of the simplified model ($I_{CaS,}$ I_{Na}) 19

Canonical model of a leech heart interneuron 27

Switching the activities between silence and bursting by a pulse of current 28

Life and death of sub-threshold oscillations 31

4 DISCUSSION 42

5 REFERENCES 47

LIST OF TABLES

Table 1: State variables operate on more than two different time scales. 4

LIST OF FIGURES

Figure 1.1: Andronov-Hopf bifurcation. 6

Figure 1.2: Saddle-node bifurcation 6

Figure 1.3: Stages of the homoclinic bifurcation in the phase plane. 7

Figure 1.4: The example of a saddle-node bifurcation for a periodic orbit. 7

Figure 3.1: Wave form of bursting activity depends on the voltage dependence of the kinetics of the fast sodium current, I_{Na}. 14

Figure 3.2: Different types of activity as Bh is varied. 15

Figure 3.3: The traces of intrinsic currents I_{Na}, I_{CaS}, inactivation h_{CaS}, and the membrane potential of the simplified model. 17

Figure 3.4: The traces of the potential for different parameters of g_{Na} are presented. 18

Figure 3.5: The model with the parameters chosen as canonical produces bursting activity which has temporal characteristics in agreement with those obtained experimentally from the leech heart interneurons isolated with bicuculline. 18

Figure 3.6: Period doubling cascade and the coexistence of chaotic spiking and bursting activity in the reduced model. 23

Figure 3.7: Coexistence of the bursting activity (blue) and the silence (green) is separated by the unstable periodic orbit at E_{leak}=-51 mV, g_{leak}=15 nS. 24

Figure 3.8: Perturbations of bursting activity by a pulse of current for the simplified model (I_{Na}, I_{CaS}). 25

Figure 3.9: Perturbation of silent regime for the simplified model (I_{Na}, I_{CaS}). 26

Figure 3.10: Series 1: Perturbation of silent regime into bursting activity. 30

Figure 3.11: Series 2: Perturbation of bursting activity into silent regime. 32

Figure 3.12: Rapid evolution of the unstable periodic orbit toward the curve of the equilibrium. 34

Figure 3.13: Dependence of the period and amplitude on g_{leak}. 35

Figure 3.14: Coexistence of the silence and bursting activities separated by unstable subthreshold oscillations. 36

Figure 3.15: Evolution of the unstable periodic orbit in the (m_{CaS}, h_{CaS}) plane and corresponding traces (V v.s t), as parameter gleak is varied. 38

Figure 3.16: Intermittent transition from bursting into silence. 39

LIST OF DIAGRAMS

Diagram 1: Bifurcation diagram of the oscillatory and stationary regimes. 20

Diagram 2: Bifurcation diagram of the canonical 14 D leech heart interneuron model. 29

Diagram 3: Area of the co-existence of bursting activity and silence is defined by the subcritical Andronov-Hopf and homoclinic bifurcation curves. 40

INTRODUCTION

Types of neuron activities

A fundamental goal of neuroscience is to understand the cellular mechanisms of neuronal network control of animal behavior. Running, swimming, breathing and other types of rhythmic motor behaviors are controlled by oscillatory neuronal networks located in the Central Nervous System (CNS) called central pattern generators (CPG) (Calabrese and Marder, 1996). Single neurons can have complex dynamics which are expressed in different types of electrical activity. The dynamics of a single neuron have to be investigated in detail to gain real understanding of the behavior of a large neuronal network.

The dynamics of a neuron are very intricate. The neuron utilizes specialized pumps and channels that operate on different time scales to create an appropriate pattern of electrical activity. This electrical activity expresses itself as the membrane electrical potential. Electrical potential across the membrane of the neuron is produced by a difference in ion concentrations between the internal and external sides of a membrane. This potential is controlled by ion channels and their conductances (Levitan and Kaczmarek, 1997). The conductance of the channels is controlled either by one variable (activation) or two variables (activation and inactivation). They are defined by slow and fast dynamics of channel sub-units. There are four main regimes of the neuronal activity: silence, sub-threshold oscillations, tonic spiking and bursting activities (Izhikevich, 1999).

1) In the silent regime, the neuron stays constantly at a certain rest potential. It does not produce spikes unless stimulated.

2) In sub-threshold oscillatory regimes, the neuron produces hyperpolarized, low amplitude oscillations of the membrane potential.
3) In the tonic spiking regime, the neuron rhythmically produces depolarized, high amplitude pulses of the membrane potential.
4) In the bursting activity regime, the neuron produces oscillatory activity which is characterized by the alternation of the tonic spiking and the silent phases.

Each of these regimes has been implicated in the control of rhythmic behaviors of animals. It has been shown that the rhythmic behaviors such as locomotion, heart beating, breathing and swimming are controlled by a Central Pattern Generator (CPG) (Arshavsky, 2002; Tryba et al., 2006; Ramirez and Viemari, 2005; Cymbalyuk and Calabrese, 2000; Cymbalyuk et al, 2002; DeLorenzo et al, 2005; Edwards et al, 1999; Hill et al, 2001; Kristan et al, 2005; Katz et al., 2004; Friesen and Stent, 1978; Arbas and Calabrese,1990, Marder and Calabrese, 1996).

Advantages of studying cellular mechanisms of neuronal dynamics in invertebrates

The main purpose of neurophysics is to understand the dynamics of neurons and neuronal networks. We think that basic mechanisms governing the dynamics are common among all animals. Invertebrates, compared to vertebrates, have much smaller Central Nervous Systems, but they are capable of producing complex patterns of behavior. The rhythmic movements of invertebrates, such as crayfish, sea slugs, crab, lobster, snail and leech, similarly to vertebrate animals (Cohen et al., 1988;Li et al 2004; Yakovenko et al., 2005; Solis et al., 2005; Lafreniere-Roula and McCrea, 2005), are controlled by CPG (Angstadt et al, 1999; Arbas et al, 1990; Arbas et al, 1984; Arshavsky et al, 1986; Arshavsky et al, 1993; DeLorenzo et al, 2005; Edwards et al, 1999, Friesen and Stent, 1978; Katz et al., 2004). The invertebrate neuronal systems provide a

number of advantages for neuroscientists. The neurons are large; some can be seen by a naked eye. The neurons can be identified, based on their location in the CNS, morphology and physiological properties, and a detailed map of the CNS can be produced. Based on these features, it is possible to assign a function for every single neuron. As a result, we can study mechanisms of neuronal control of a behavior on a cellular level.

The medicinal leech's CNS is relatively well studied. Neurobiological investigation has been focused on the seven types of rhythmical behavior: heartbeating, crawling, swimming, feeding, shortening and local bending and decision making (Angstadt et al., 1999; Arbas et al., 1990; Arbas et al, 1984; Cymbalyuk et al., 2000; Hill et al., 2001; Kristan et al., 2005, Friesen and Stent, 1978; Simon et al.,1994). The nervous system of the leech includes 21 segmental ganglia. Approximately, each segmental ganglion contains 400 neurons and most of them are paired. The knowledge of morphology and physiological properties allows one to study the behavior of the leech and to correlate it with a motor pattern. One of the best studied rhythmic behaviors of the leech is the heart beating (Calabrese et al., 1995; Masino and Calabrese, 2002). The heartbeat CPG has been identified. It is controlled by paired neurons in the first four segmental ganglia (Kristan et al, 2005 ; Hill et al, 2001). Two pairs of mutually inhibitory heart interneurons, which are located in the third and fourth ganglia, create two elemental oscillators. Each pair of neurons is known as an elemental oscillator. As the extracellular recoding shows, a heartbeat interneuron can produce endogenous rhythmic bursting when it is isolated with bicuculline (Cymbalyuk et al., 2002).

We analyze a model of the leech heart interneuron, developed by Hill et al., (2001). A neuron is represented as a single isopotential compartment with Hodgkin-Huxley type membrane conductances (Huxley, 2002). It is described by a system of nonlinear differential equations. The

leech heart interneuron contains eight voltage-dependent currents. Five of them are inward currents: a transient, fast sodium (Na^+) current (I_{Na}); a persistent Na^+ current (I_P); a fast, low-threshold calcium (Ca^{2+}) current (I_{CaF}); a slow, low-threshold Ca^{2+} current (I_{CaS}); and a hyperpolarization-activated cation current (I_h) (Opdyke and Calabrese, 1994; Olsen et al., 1995; Olsen and Calabrese, 1996; Angstadt and Calabrese, 1989, 1991). Three outward currents are: a delayed rectifier-like potassium (K^+) current (I_{K1}); a persistent K^+ current (I_{K2}), and a fast, transient K^+ current (I_{KA}) (Hill et al, 2001; Nadim and Calabrese, 1997).The kinetics, voltage dependency, and reversal potentials of these currents are described in the Methods. The model is tuned to produce the activity with characteristics such as period, duty cycle and frequency of bursting activity tuned to the experimental data (Hill et al, 2001; Cymbalyuk et al., 2002).

As we mentioned above, our particular interest is to understand the dynamics of the leech heart interneuron model leading to the co-existence of bursting and silence. We envisage a neuron as a multidimensional dynamical system. The dynamics of the model are described by a 14 dimensional system of differential equations. The kinetics of the currents operate on different time scales. Activations and inactivations were identified as ultra fast, fast, moderate, slow and very slow (Table 1) (Cymbalyuk et al, 2003).

Table 1. State variables operate on more than two different time scales. Some of the state variables have a different time scale depending on the membrane potential (marked by red in the table).

	from -70 mV to -50 mV	from -50 mV to -10 mV
Ultra fast (0.1 msec)	m_{Na}	m_{Na}
Fast (~2-10 msec)	h_{Na}, m_{K1}, m_{CaF}, m_{CaS}	m_P, m_{KA}, h_{Na}, m_{K1}, m_{CaF}
Moderate (~100 msec)	h_{KA}, m_{K2}, m_P, m_{KA}	m_{CaS}, h_{CaF}, h_{KA}, m_{K2}
Slow (~ 0.5 sec)	h_{K1}, h_{CaS}, h_{CaF}	h_{K1}
Very Slow (~ 2-6 sec)	m_h	h_{CaS}, m_h

The complexity of endogenous dynamics originates from dynamical diversity of ionic currents

which can be separated by different time scales and other characteristics (see Table 1). Analysis in terms of fast-slow dynamical systems gives insight into the mechanisms responsible for the generation of bursting behavior.

Bifurcations in the model and the transitions between different types of electrical activities

The leech heart interneuron model can produce complex dynamics. Most of the dynamical behaviors of this model can be reproduced in the simplified models. There are four types of bifurcations (transition mechanisms) which are common for nonlinear dynamical systems like Hodgkin-Huxley type models: Andronov-Hopf bifurcation, Saddle-node bifurcation for an equilibrium, Homoclinic bifurcation, and Saddle-node bifurcation of a periodic orbit (Guckenheimer and Tein, 2003). These bifurcations play the key roles in controlling transitions between behaviors in the neuronal models.

1) Andronov-Hopf bifurcation describes the emergence of a periodic orbit from an equilibrium state. At this bifurcation the stationary states has a pair of purely imaginary characteristic exponents. There are two types of the Andronov-Hopf bifurcation: sub-critical and super-critical. Figure 1.1(a) illustrates the super-critical bifurcation where a stable periodic orbit with zero amplitude emerges from the equilibrium state in the phase plane. In contrast, at the sub-critical bifurcation an unstable periodic orbit collapses at the equilibrium state (see Figure 1.1(b)). (Shilnikov et al, Vol 1-2 , 2001)

2) Saddle-node bifurcation describes the metamorphosis of an equilibrium state with a single zero characteristic exponent. Here, the stable and unstable states move closer to each other, then merge and disappear (Figure 1.2) (Guckenheimer and Tein, 2003; Strogatz , 1998; Shilnikov et al., 2001).

3) Homoclinic bifurcation: the stable and unstable separatrices of a saddle point form a closed orbit called the homoclinic loop. Through a homoclinic bifurcation a periodic orbit disappears as it merges into the homoclinic loop (Figure 1.3); note that its period grows without an upper bound (Shilnikov et al, 2001 ; Strogatz, 1998).

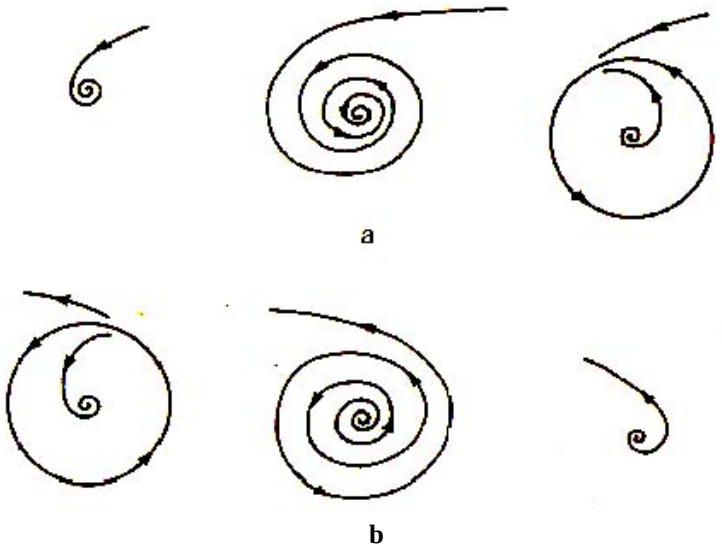

Figure 1.1: Andronov-Hopf bifurcation. a) The supercritical and b) subcritical Andronov-Hopf bifurcations are illustrated. (the figure is taken from Strogatz, 1998)

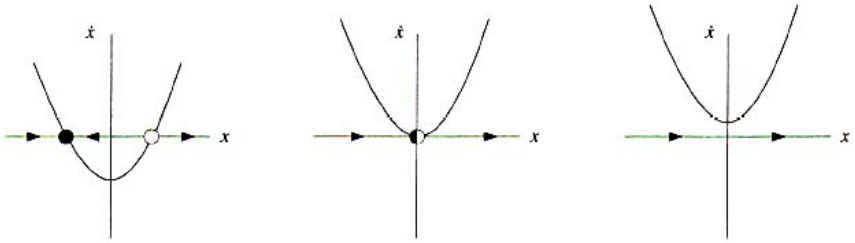

Figure 1.2: Saddle-node bifurcation (the figure is taken from Strogatz, 1998).

4) Saddle-node bifurcation of a periodic orbit (also called fold) - a stable periodic orbit and unstable periodic orbit coalesce and annihilate (see Figure 1.4) (Shilnikov et al, 2001; Strogatz, 1998).

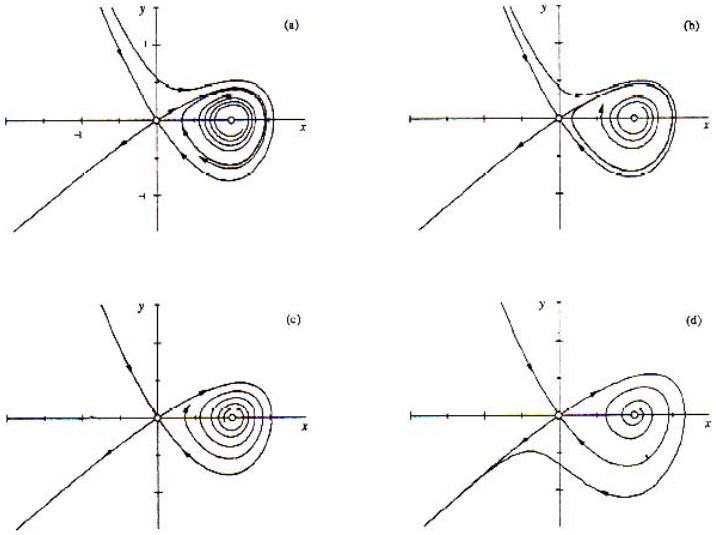

Figure 1.3: Stages of the homoclinic bifurcation in the phase plane. A bifurcation parameter x changes. (a) For x< x', a stable periodic orbit passes closer to a saddle point at the origin. As x increases to x', the periodic orbit swells (b) and collides with a saddle, creating a homoclinic orbit or loop (c). For x> x', the saddle connection breaks and the homoclinic orbit is destroyed (d) (figure is taken from Strogatz, 1998).

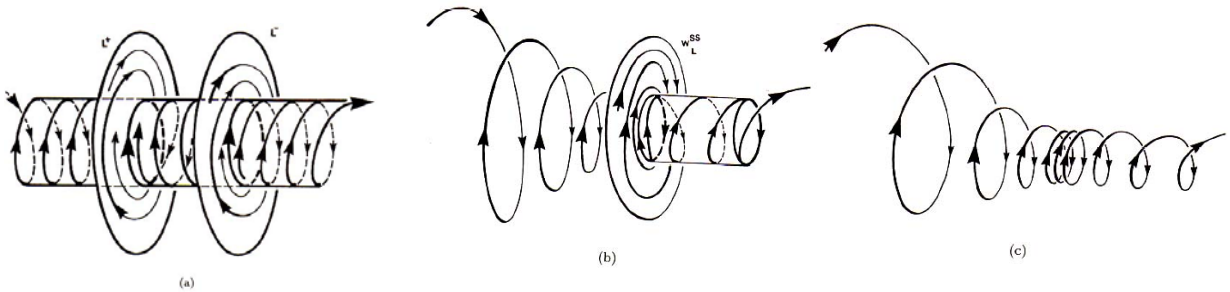

Figure 1.4: The example of a saddle-node bifurcation for a periodic orbit. (a) As bifurcation parameter x is varied, the stable and unstable periodic orbits stay close to each other, (b) for x =x', the two orbits coalesce and (c) for x >x', the periodic orbits disappear (figure is taken from Shilnikov et al, 2001).

METHODS

We analyze a single compartment model of a leech heart interneuron (Hill et al.,2001; Cymbalyuk et al., 2002). The solutions of this model were obtained using Matlab ODES solvers. The integration and bifurcation analysis were performed using the software package CONTENT, developed for the bifurcation analysis of dynamical systems. Content is freely available at http://www.cwi.nl/ftp/CONTENT. Integration of equations was done using the Runge-Kutta method of the 4-th order with the minimal step size and tolerance of integration set as 10^{-14} and 10^{-9} correspondingly.

A leech heart interneuron is modeled as a single isopotential compartment with membrane conductances represented in terms of the Hodgkin and Huxley formalism (Huxley, 2002). The dynamics of membrane potential (V) of a neuron are described by

$$C\frac{dV}{dt} = -(I_{Na} + I_P + I_{CaF} + I_{CaS} + I_h + I_{K1} + I_{K2} + I_{KA} + I_{leak} + I_{pulse}(t)),$$

where C is the total membrane capacitance (0.5 nF), I_{ion} is an intrinsic voltage-gated current, I_{pulse} is the injected current and I_{Leak} is the leak current. The voltage-gated currents are given by

$$I_{Na} = \bar{g}_{Na} m_{Na}^3 h_{Na} (V - E_{Na}); \; I_P = \bar{g}_P m_P (V - E_{Na}); \; I_{CaF} = \bar{g}_{CaF} m_{CaF}^2 h_{CaF} (V - E_{Ca});$$

$$I_{CaS} = \bar{g}_{CaS} m_{CaS}^2 h_{CaS} (V - E_{Ca}); \; I_{K1} = \bar{g}_{K1} m_{K1}^2 h_{K1} (V - E_K); \; I_{K2} = \bar{g}_{K2} m_{K2}^2 (V - E_K);$$

$$I_{KA} = \bar{g}_{KA} m_{KA}^2 h_{KA} (V - E_K); \; I_h = \bar{g}_h m_h^2 (V - E_h); \quad I_{leak} = \bar{g}_{leak} (V - E_{leak}); \; I_{pulse}(t) = I_{pulse} f(t_{pulse});$$

where $\overline{g}_{ion}$ is the maximal conductance, E_{ion} is the reversal potential, $f(t_{pulse})$ is 1 during the pulse time, otherwise $f(t_{pulse})$ is 0, m and h are the activation and inactivation variables, respectively. These variables are governed by the following equations

$$\frac{dm_{K2}}{dt} = \frac{f_{\infty}(-83, 0.02, V) - m_{K2}}{\tau(200, 0.035, 0.057, 0.043, V)}$$

$$\frac{dm_{P}}{dt} = \frac{f_{\infty}(-120, 0.039, V) - m_{P}}{\tau(400, 0.057, 0.01, 0.2, V)}$$

$$\frac{dm_{Na}}{dt} = \frac{f_{\infty}(-150, 0.029, V) - m_{Na}}{0.0001}$$

$$\frac{dh_{Na}}{dt} = \frac{f_{\infty}(500, 0.030, V) - h_{Na}}{\tau_{hNa}(V)}$$

$$\frac{dm_{CaF}}{dt} = \frac{f_{\infty}(-600, 0.0467, V) - m_{CaF}}{\tau_{mCaF}(V)}$$

$$\frac{dh_{CaF}}{dt} = \frac{f_{\infty}(350, 0.0555, V) - h_{CaF}}{\tau(270, 0.055, 0.06, 0.31, V)}$$

$$\frac{dm_{CaS}}{dt} = \frac{f_{\infty}(-420, 0.0472, V) - m_{CaS}}{\tau(-400, 0.0487, 0.005, 0.134, V)}$$

$$\frac{dh_{CaS}}{dt} = \frac{f_{\infty}(360, 0.055, V) - h_{CaS}}{\tau(-250, 0.043, 0.2, 5.25, V)}$$

$$\frac{dm_{K1}}{dt} = \frac{f_{\infty}(-143, 0.021, V) - m_{K1}}{\tau(150, 0.016, 0.001, 0.011, V)}$$

$$\frac{dh_{K1}}{dt} = \frac{f_{\infty}(111, 0.028, V) - h_{K1}}{\tau(-143, 0.013, 0.5, 0.2, V)}$$

$$\frac{dm_{KA}}{dt} = \frac{f_{\infty}(-130, 0.044, V) - m_{KA}}{\tau(200, 0.03, 0.005, 0.011, V)}$$

$$\frac{dh_{KA}}{dt} = \frac{f_{\infty}(160, 0.063, V) - h_{KA}}{\tau(-300, 0.055, 0.026, 0.0085, V)}$$

$$\frac{dm_h}{dt} = \frac{f_{h\infty}(V) - m_h}{\tau(-100, 0.073, 0.7, 1.7, V)}$$

where the steady-state activation and inactivation functions are given by Boltzmann function

$$f_{\infty}(a,b,V) = \frac{1}{1+e^{a(V+b)}}$$

except for the steady-state activation of I_h which is given by

$$f_{h\infty}(V) = \frac{1}{1+2e^{180(V+0.047)}+e^{500(V+0.047)}}$$

The time constants are also described by the following a Boltzmann function, except for the inactivation time constant for I_{Na}, the activation time constant for I_{KF}, and the activation time constant for I_{CaF}

$$\tau(a,b,c,d,V) = c + \frac{d}{1+e^{a(V+b)}}$$

$$\tau_{hNa}(V) = 0.004 + \frac{0.006}{1+e^{500(V+0.028)}} + \frac{0.01}{\cosh(300(V+0.027))}$$

$$\tau_{mKF}(V) = 1.5 + \frac{8.0}{1+e^{-100(V+0.022)}} + \frac{-2.2}{\cosh(100(V+0.04))}$$

$$\tau_{mCaF}(V) = 0.011 + \frac{0.024}{\cosh(-330(V+0.0467))}$$

The canonical parameter values are set as follows:

the reversal potentials are E_{Na}=-0.045 V, E_{CaS}=0.135 V, E_K=-0.07 V, E_h=-0.021 V, and the maximal conductances for the elemental oscillator neurons are $\bar{g}_{Na}$=200 nS, $\bar{g}_P = 7$ nS, $\bar{g}_{CaF} = 5$ nS, $\bar{g}_{CaS} = 3.2$ nS, $\bar{g}_{K1} = 100$ nS, $\bar{g}_{K2} = 80$ nS, $\bar{g}_{KA} = 80$ nS, $\bar{g}_h = 4$ nS, $\bar{g}_l = 8$ nS.

Next, we will describe a simplified leech neuron model, which is based on the fast sodium and slow calcium voltage-dependent currents and the leak current.

This model has four equations. We assume that the activation for I_{Na} is instantaneous, therefore $m_{Na} = f_\infty(-150,0.028,V)$.

The dynamics of the membrane potential, V, activation (m) and inactivation (h) variables of the sodium and calcium currents in this model are described by:

$C dV/dt = -(\bar{g}_{Na} f_\infty^3(-150, 0.028, V) h_{Na}(V-E_{Na}) + \bar{g}_{CaS} m^2_{CaS} h_{CaS}(V-E_{CaS}) + g_{leak}(V-E_{leak})) + I_{pulse}(t)$;

$$\frac{dh_{Na}}{dt} = \frac{f_\infty(500, Bh, V) - h_{Na}}{\tau_{hNa}(V)}$$

$$\frac{dm_{CaS}}{dt} = \frac{f(-420,0.0472,V) - m_{CaS}}{\tau(-400,0.00487,0.005,0.134,V)}$$

$$\frac{dh_{CaS}}{dt} = \frac{f(360,0.055,V) - h_{CaS}}{\tau(250,0.043,0.02,5.25,V)}$$

Here the parameters are: $\bar{g}_{CaS}$=80 nS, $\bar{g}_{Na}$=250 nS, and Bh=0.031V. The function $f_\infty(a,b,V)$ is the Boltzmann function $f=1/(1+e^{a(V+b)})$. In the simplified model the parameter Bh produces a shift of the steady-state inactivation curve of I_{Na} relative to the potential V in the equation $\frac{dh_{Na}}{dt} = \frac{f_\infty(500, Bh, V) - h_{Na}}{\tau_{hNa}(V)}$.

RESULTS

Simplified model

Our main goal is to understand the dynamics of the leech heart interneuron. Our study is primarily focused on understanding the mechanisms underlying the co-existence of the bursting and silent regimes. Because the dynamics of the complete model of the 14 state variables is very complex, we simplified it first by reducing the number of the equations. A primary advantage of creating such a simplified model of the interneuron is that the analysis of this model will be more comprehensive. The minimal order of the model is determined by our fundamental knowledge of the processes underlying the onset of the principal activities of neurons such as bursting and tonic spiking. Our modeling approach is based on the theory of slow-fast dynamical systems (Rinzel et al., 1985; Bedrov et al., 2000; Belykh et al., 2000; Izhikevich et al., 2000; Cymbalyuk et al., 2003; Shilnikov et. al., 2003; Shilnikov et al., Vol. 1-2, 2001). The slowest variable controlling the burst duration in the complete model is the inactivation of I_{CaS} (Hill et al., 2000; Cymbalyuk, et al., 2003; Olypher et al., 2006). It has been suggested that I_{CaS} underlies the bursting activity (Cymbalyuk et. al. 2003). The numerical experiment performed on the complete model has revealed that if I_{Na} is blocked, the model produces oscillatory activity (Cymbalyuk et al., 2003). Our minimal model is based on the slow calcium current, the fast sodium current and the leak current. The current I_{Na} exhibits an ultra fast activation and determines the fast spiking dynamic (see Table 1). The dynamics and contributions of all other currents are not considered. Note that the simplified model based on (I_{Na}, I_{CaS}) does not have the outward currents, except for $I_{leak,}$ so the balance of inward and outward currents is lost. Usability of this model depends on whether it could produce the bursting activity with temporal characteristics similar to those

experimentally observed in the leech heart interneuron. To determine these proper parameters values (called canonical) for the simplified model, we varied, systematically, the maximum conductance $\overline{g}_{ion}$, and the activation and inactivation kinetics for I_{CaS} and I_{Na}.

Window current mode of I_{Na}

The steady-state activation and inactivation curves of I_{Na} are described by the Boltzmann function; they characterize the kinetics of ion currents. When all channels are open, then the ion current has the maximum conductance $\overline{g}_{ion}$. The product of $\overline{g}_{ion}$, activation and inactivation gives the instantaneous conductance. The shift of the inactivation curve relative to the activation curve changes the steady-state conductance of I_{Na}. For example, if the potential is fixed to a hyperpolarized value, then activation equals 0 while the inactivation equals 1; therefore the steady-state conductance g_{ion}^{∞} is 0. Similarly, if the potential is fixed to the depolarized value, the activation equals 1 and the inactivation equals 0, so g_{ion}^{∞} is 0 as well. It is important to note that for certain kinetics of activation and inactivation curves, there is a "window" interval in the values of the membrane potential where g_{ion}^{∞} is non-zero. We can determine the "window" sodium current as a steady-state current at a membrane potential in the "window" interval, near the voltage the steady-state curves for activation and inactivation intersect (see Figure 3.1). As Figure 3.1 (A) shows, for some range of voltage around -0.032 V the steady-state conductance g_{Na}^{∞} is not zero. If the membrane potential is fixed within the "window", then the current I_{Na} is persistent. In the simplified model, the "window" current plays the role similar to that of the sodium persistent current, which supports burst duration in the complete model (Hill et al, 2001; Cymbalyuk and Calabrese, 2001)

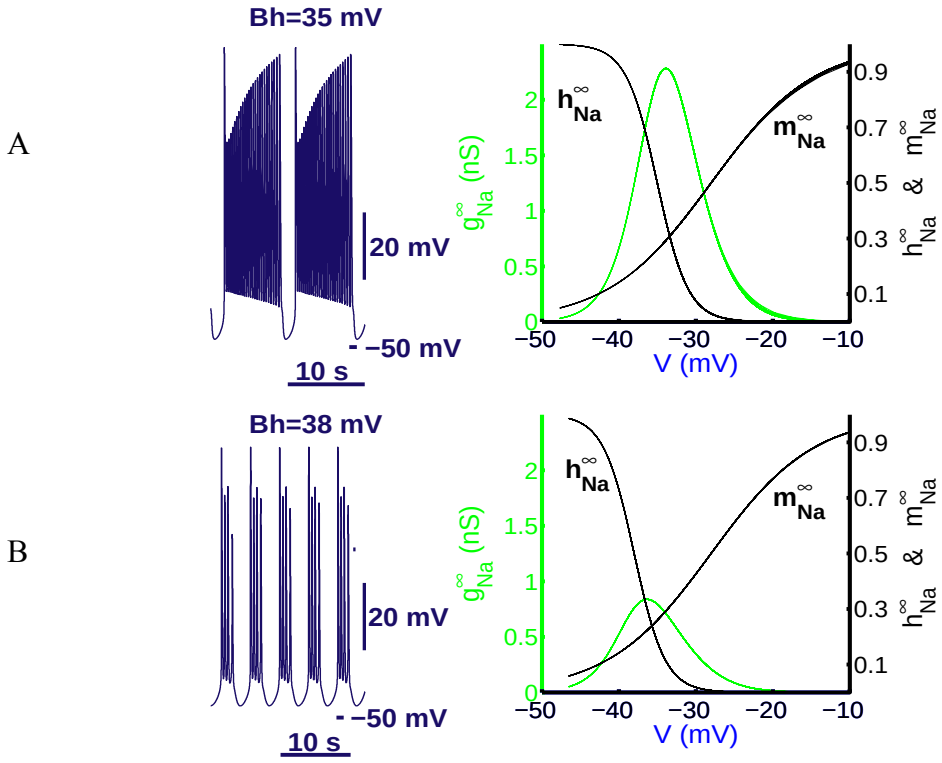

Figure 3.1. Wave form of bursting activity depends on the voltage dependence of the kinetics of the fast sodium current, I_{Na}. The data are presented for two different values of Bh, which shifts the steady state inactivation curve, for Bh =0.035 V at the top row and for Bh=0.038 V at the bottom one. The increase of Bh shifts the curve towards the hyperpolarized values and changes the steady state conductance g^{∞}_{Na}. On the left panels the bursting waveforms are presented. On the right side there are corresponding graphs of the steady-state activation, m^{∞}_{Na}, and inactivation, h^{∞}_{Na}, curves presented in black and the steady-state conductance, g^{∞}_{Na}, presented in green. The overall decrease of g^{∞}_{Na} decreases the period, burst duration and duty cycle of the model. The ratio of the maximum values of g^{∞}_{Na} calculated for the two values of Bh equals $g^{\infty}_{Na,Bh=0.035} / g^{\infty}_{Na,Bh=0.038}$ =2.7

Canonical parameters of model (I_{CaS}, I_{Na}).

To tune up the period and the burst duration of the simplified model to the values corresponding to the experimental data, we need to explore the dynamics of I_{Na}. We introduce the parameter Bh defined as the half-inactivation voltage in the Boltzmann function

$f(V)=1/(1+e^{500(V+Bh)})$ which defines the steady-state condition for h_{Na}^{∞}. Let's consider how the activity of the neuron changes as Bh shifts toward hyperpolarized values. As its value is increased (see Figure 3.1), this shifts the curve h_{Na}^{∞} towards the hyperpolarized values. As Bh increases, the period of bursting activity decreases. The analysis of the results (see Figure 3.2) shows that the variations of Bh affect the conductance of $I_{Na,}$ which alters the model activity. For Bh=0.04 V, the model is in the silent regime. As Bh decreases from 0.037 V to 0.035 V, the period of bursting activity grows. This leads to the increase of the burst duration (from 5.4 sec to 9.2 sec), spike frequency (from 2.7 Hz to 4.4 Hz) and duty cycle (from 52.4 % to 78%), while

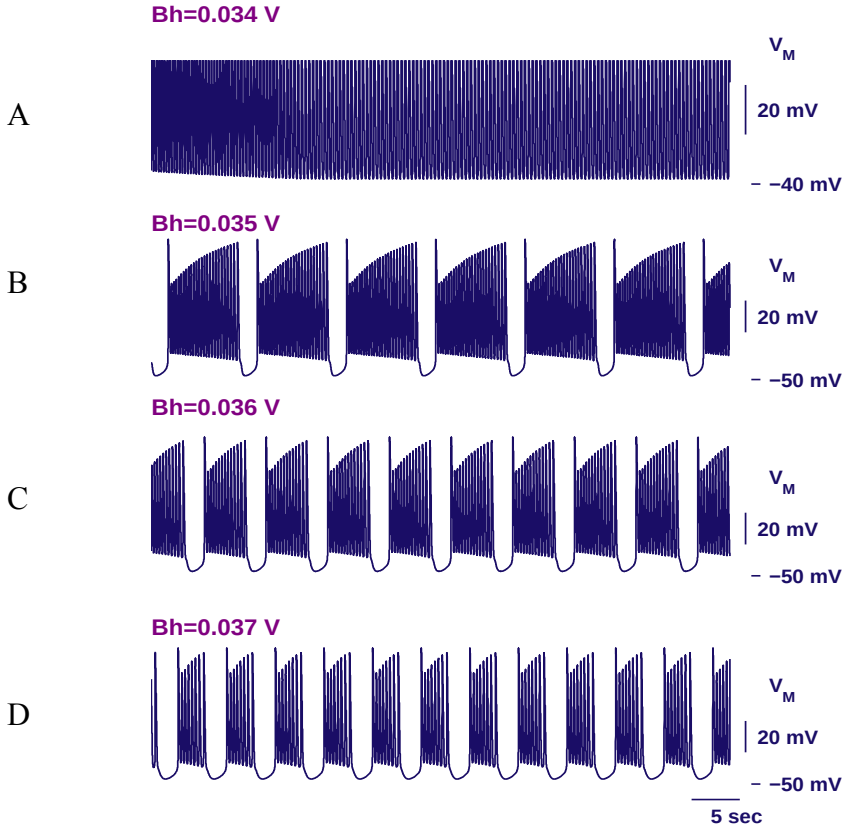

Figure 3.2. Different types of activity as Bh is varied. A) at Bh=0.034 V, the model demonstrates tonic spiking activity. B) Bh=0.035 V, it shows the bursting activity with the following characteristics: Period P=9.2 sec, Spike Frequency F=4.4 Hz, Duty Cycle D=78%. C) Bh=0.036 bursting activity with characteristics P=6.4s, F=3.6Hz, D=64.8%, similar to the experimental data that was obtained. D) Bh=0.037 V corresponds to the bursting activity with P=5.4 s, F=2.7 Hz; D=52.4 %.

the interburst interval stays nearly same. The model (I_{Na}, I_{CaS}) at Bh=0.034 V shows the depolarized tonic spiking activity presented in Figure 3.2 A

We suggest in this model that the activation of I_{CaS} initiates the beginning of spikes of bursting activity, while inactivation of I_{CaS} controls the burst duration similar to half-center oscillator created of two heart interneuron (Olypher et al., 2006; Li et al.,1997). To analyze the dynamics of I_{CaS} current in the simplified mode, we plot I_{Na} and I_{CaS} currents during bursting activity. As Figure 3.3 shows, the burst duration of the model is indeed determined by the slow inactivation, h_{CaS}. During the quiescence phase, I_{CaS} activates, thereby depolarizing the neuron, and leads to the transition into the burst phase. The window mode of I_{Na} supports the burst along with I_{CaS}. This result agrees with the results in Hill et al. (2002) and Olypher et al. (2006).

To compare the dynamics of the simplified model and that of the complete model, we block I_{Na}, in the simplified model, and observe slow voltage oscillations induced by the dynamic of I_{CaS} (Figure 3.4). These oscillations are sustained in both the presence and absence of I_{Na}. Similar results are shown in the complete model (Cymbalyuk et al. 2003). As we vary the maximum conductance $\bar{g}_{Na}$, we observe at $\bar{g}_{Na}$=110 nS that the model shows bursting activity with a single large spike followed by a plateau. The period of the bursting activity is slightly longer than the period of I_{CaS}. For parameters $\bar{g}_{Na}$=220 nS and $\bar{g}_{Na}$=250 nS the period equals 6.6 sec and 7.6 sec, correspondingly. Both examples have a short plateau at the beginning of the burst (see Figure 3.4). This plateau is associated with the window in I_{Na} and dynamics I_{CaS}.

This analysis of the dynamics of the currents allows us to adjust the proper parameters for the simplified model, which we have called canonical, so the model can exhibit activities with characteristics similar to experimental data. To change the interburst interval in the simplified model, we varied the characteristics of I_{CaS}. To modify the burst duration and spike frequency,

the dynamics of the inactivation and activation of I_{Na} have to be adjusted as well. The simplified model with parameters $\bar{g}_{Na}$ =250 nS, $\bar{g}_{CaS}$ =80 nS , and Bh=0.031 V shows bursting activity with period and duty cycle similar to the experimental characteristics of the bursting activity of a leech heart interneuron (see Figure 3.5). The temporal characteristics of this activity were recorded extracellularly from the leech heart interneuron (Cymbalyuk et al., 2002). Other parameters of the simplified model are described in Methods.

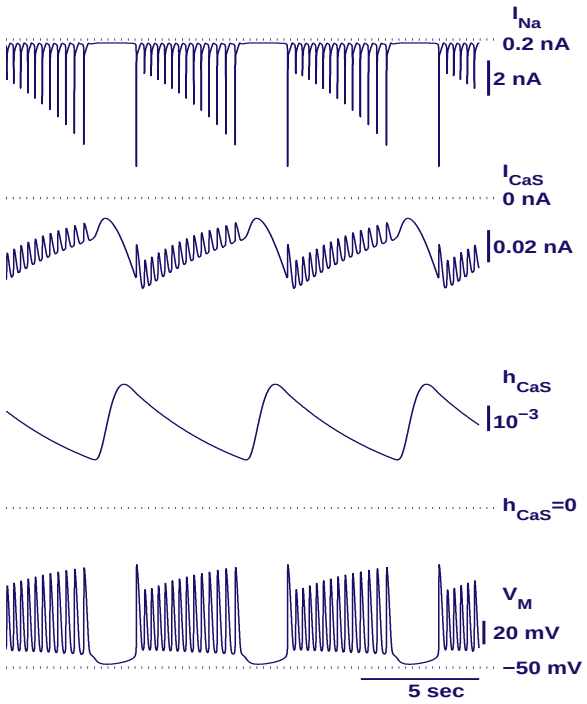

Figure 3.3 The traces of intrinsic currents $I_{Na,}$ I_{CaS}, inactivation $h_{CaS,}$ and the membrane potential of the simplified model. During the quiescence phase of bursting activity, I_{CaS} activates, it depolarizes the neuron, and leads to the transition into the burst phase. Once the burst has begun, it is sustained primarily by $I_{Na.}$. Here, the bursting activity has the period P=6.5 sec and duty cycle D=65.4% closed to the experimental data (Cymbalyuk et.al. 2002).

As we mentioned above, the main question here is whether the simplified model, with properly set canonical parameters, can also demonstrate the co-existence of bursting activity and silent regimes that was found in the original leech heart interneuron model.

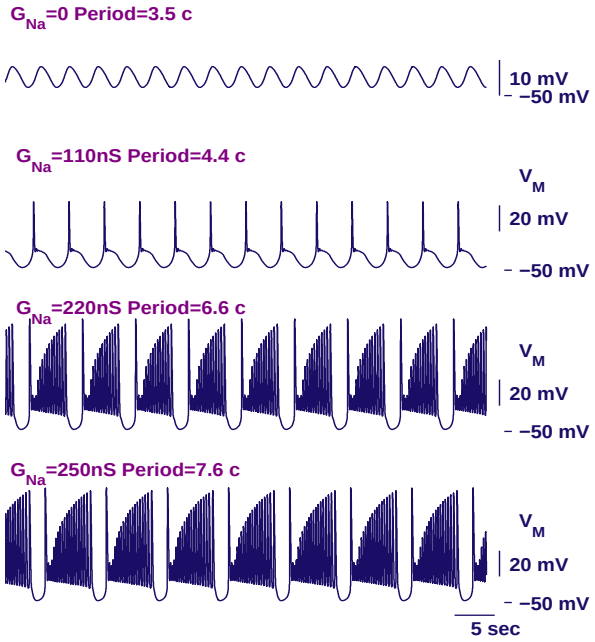

Figure 3.4. The traces of the potential for different parameters of $\bar{g}_{Na}$ are presented. For $\bar{g}_{Na}$ =0, the model shows oscillations. An increase of $\bar{g}_{Na}$ leads to the onset of the bursting activity. For $\bar{g}_{Na}$ =110 nS, the bursting activity with plateau is initiated. As $\bar{g}_{Na}$ is increased from 220 nS to 250 nS, the period increases.

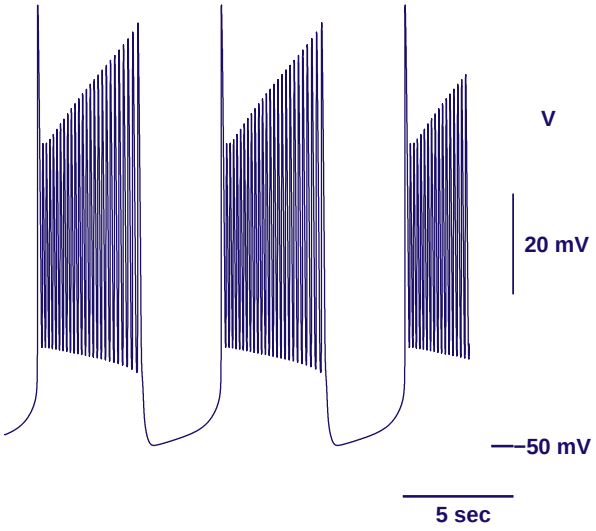

Figure 3.5 The model with the parameters chosen as canonical produces bursting activity which has temporal characteristics, period and burst duration, in agreement with those obtained experimentally from the leech heart interneurons isolated with bicuculline. Here, Period is 8.3 sec and Duty Cycle is 54 %, Frequency =5.9 Hz, Interburst Interval =3.8 sec. Canonical parameters here and below are: E_{leak} =-0.0505 V, g_{leak} =15.7 nS, $\bar{g}_{CaS}$ =80 nS; E_{Ca}=0.135 V; $\bar{g}_{Na}$ =250 nS; E_{Na}=0.045 V; Bh=0.031 V.

Moreover, if it does, what are the mechanisms supporting this bi-stability?

Bifurcation analysis of the simplified model (I_{Na}, I_{CaS})

The next step is to find this co-existence in the simplified model. The bifurcation analysis is the key element that helps us predict and localize the co-existence area in the parameter space. The previous studies have confirmed that the full model is quite sensitive to leak current parameters (g_{leak}, E_{leak}) (Cymbalyuk et al., 2002). We have numerically computed similar bifurcation diagram of oscillatory and stationary states (see Diagram 1). This diagram describes the transitions between the activities that could occur in the reduced model. Our numerical analysis of the neuron model is done using Content. We have determined the areas of hyperpolarized and depolarized silence (a steady stationary state), the areas of tonic spiking (a stable periodic orbit) and bursting activity, and the area of multistability. As mentioned above, the following four types of bifurcations predict these oscillatory and stationary state areas, namely: the Andronov-Hopf and the saddle-node bifurcations of equilibrium states, and the homoclinic and saddle-node bifurcations of periodic orbits.

To locate the parameter domain corresponding to the bursting activity in the parameters plane for the four dimensional simplified (I_{Na}, I_{CaS})- model, we have analyzed the stability of the hyperpolarized stationary state. The equilibrium state conditions are:

1) $CdV/dt = 0;\ \frac{dh_{Na}}{dt} = 0;\quad \frac{dm_{CaS}}{dt} = 0;\quad \frac{dh_{CaS}}{dt} = 0;$

The corresponding time-constant solution of the system with respect to activation and inactivation of the model is given by

$f_{\infty}(500, 0.03, V) = h_{Na}$;

$f_{\infty}(-420, 0.0427, V) = m_{CaS}$; $\Rightarrow$

$f_\infty(360,0.055,V) = h_{CaS}$;

$g_{Na}m^3{}_{Na}h_{Na}(V\text{-}E_{Na})+ g_{CaS}\,m^2{}_{CaS}h_{CaS}(V\text{-}E_{CaS}) +g_{leak}(V\text{-}E_{leak})=0;$

The values m_{CaS}, h_{CaS} and h_{Na} are then substituted into the equation

$g_{Na}\ \ f_\infty(\ -150, 0.028, \mathrm{V})^{\,3}\ f_\infty(500,0.03,V)(V\text{-}E_{Na})+g_{CaS}\ \ f_\infty(-420,0.0427,V)^{\,2}\ f_\infty(360,0.055,\mathrm{V})(V\text{-}E_{CaS}) +g_{leak}(V\text{-}E_{leak})=0$, where $g_{Na,}$ g_{CaS} and E_{Na}, E_{CaS}, E_{leak} are given values.

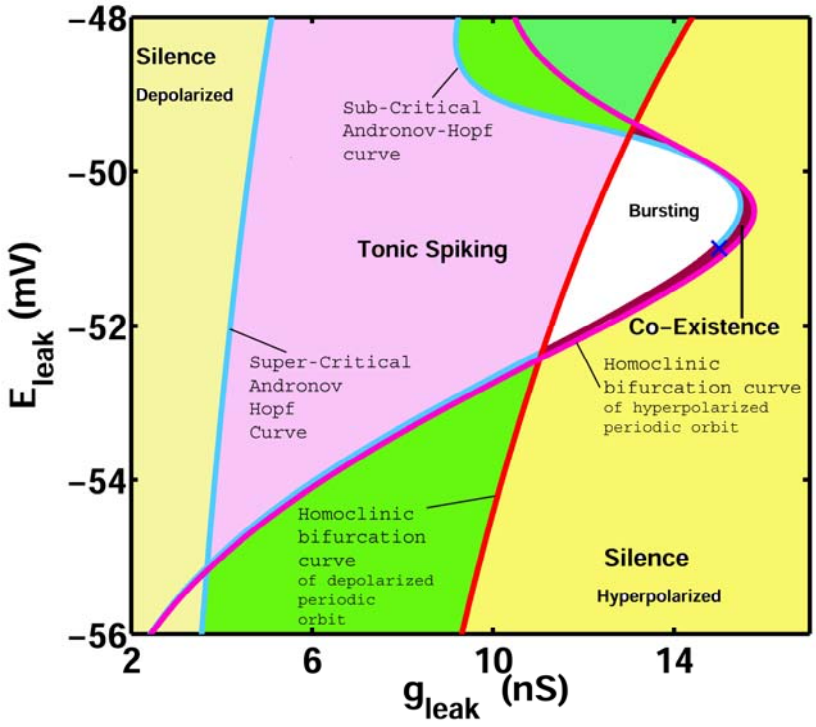

Diagram 1. Bifurcation diagram of the oscillatory and stationary regimes. The Andronov-Hopf bifurcation of the hyperpolarized stationary state (silent regime) is shown by the blue curve and marks the boundary where silent regime loses stability giving rise to the subthreshold oscillations. The other blue curve marks Andronov-Hopf bifurcation of the depolarized stationary state. At this curve depolarized stationary state loses stability and gives rise to a periodic tonic spiking. The red curve locates homoclinic bifurcation of the large amplitude periodic spiking. The pink curve corresponds to the homoclinic bifurcation of the unstable sub-threshold oscillations. The area between these curves of homoclinic bifurcations is the parameter regime where bursting is observed, marked in the white. The area between the blue and the pink curves marks the parameter regime where unstable sub-threshold oscillations exist; this is parameter regime of bi-stability of silence and bursting. The blue x on the area of co-existence marks parameters used for Figures 3.7.

It allows us to calculate the so-called equilibrium curve in the (V, g_{leak})-plane. Let us point out that the periodic orbit emerges from the equilibrium point through the Andronov-Hopf bifurcations. When born, the periodic orbit has zero amplitude and some non-zero period. As the bifurcation parameter g_{leak} is varied, the amplitude grows proportionally to $\sqrt{g_{leak} - g^{o}_{leak}}$, where g^{o}_{leak} is the bifurcation value, while its period is evaluated as T=2π/ω, where the frequency ω is the imaginary part of the characteristic exponents. Writing down the Jacobian J(V,m_{CaS}, h_{CaS}, h_{Na}) for the four dimensional model, we determine the conditions for the Andronov-Hopf bifurcation as $Tr(J) = 0$ and $Det(J)$>0, the real parts of a pair of eigenvalues must cross zero at the bifurcation value. Solving the system of equations gives us the set of the eigenvalues (λ) which characterize the Andronov-Hopf bifurcation. The imaginary part of λ defines the frequency, ω, of the newborn periodic orbit. There is a "Lyapunov" quantity found through the third degree Taylor expansion of the vector field at each Andronov-Hopf bifurcation point which determines the stability of the periodic orbits. The Lyapunov quantity for the super-critical Andronov-Hopf bifurcation is negative, therefore the periodic orbit is born stable. At the sub-critical Andronov-Hopf bifurcation, the Lyapunov quantity is positive and the periodic orbit is born unstable (Guckenheimer , 2003; Shilnikov et. al., Vol 1-2, 2001).

One can see the super-critical Andronov-Hopf bifurcation curve in Diagram 1. This curve corresponds to the transition from depolarized silence into tonic spiking activity. As the parameter g_{leak} is increased, the stable periodic orbit moves toward the saddle equilibrium.

The coordinates of the saddle equilibrium are given by $m^{\bullet}_{CaS} = h^{\bullet}_{CaS} = h^{\bullet}_{Na} = V^{\bullet} = Det(J) = 0$. Before the stable periodic orbit comes close to the saddle equilibrium, it becomes unstable through the period doubling bifurcation. For example, at g_{leak}=4.66 nS and E_{leak}=-52 mV the stable periodic orbit has the frequency ω=51.8 rad/sec. As

g_{leak} increases, its amplitude grows proportionally to $\sqrt{g_{leak} - 4.66}$. The periodic orbit loses stability at g_{leak}= 12 nS. Then, for a small change in g_{leak}, the period grows fast and logarithmically. When the trajectory becomes the homoclinic orbit to the saddle equilibrium, the tonic-spiking activity ceases.

The homoclinic bifurcation curve in the two parameter plane was computed using Content. We use the fact that the period of the tonic spiking orbit increases unboundedly, so we were able to detect an isochrone corresponding to the period of 50 sec, which gives a good approximation for the homoclinic bifurcation. This curve (the red) in Diagram 1, determines the transition from the tonic spiking into bursting activity in the reduced model.

On the other hand, for g_{leak}=12.2 nS the unstable periodic orbit bifurcates from the hyperpolarized stationary state through the sub-critical Andronov-Hopf bifurcation with the frequency ω=2.3rad/sec. Content allows us to continue the Andronov-Hopf bifurcation as two parameters are varied; its curve is shown in Diagram 1. Similarly, as the parameter g_{leak} is increased, the unstable sub-threshold periodic orbit gets closer to the saddle equilibrium. When g_{leak}=12.5 nS, the period of its oscillations grows unboundedly, while its amplitude remains finite. At the critical parameter value of $g_{leak,}$ the periodic orbit collides with the saddle equilibrium and the oscillations vanish. The corresponding bifurcation curve is shown by the pink curve in Diagram 1. This curve determines the transition between the bursting and the silent regimes.

As the results of the dynamical systems analysis suggest, the transitions between different types of model activity can be identified by the means of bifurcation theory. Crossing a bifurcation boundary in the model is associated with some qualitative change in the oscillatory properties of a neuron. 1) The transition from tonic spiking into bursting activity is associated

with a period doubling cascade leading into chaos in the model. This transition is illustrated in Figure 3.6. The cascade of period doubling bifurcations leading to chaos is observed in the simplified model. This cascade also persists in the original model of a leech heart interneuron (Cymbalyuk et al. 2002). A narrow area near the transition border corresponds to that of the co-existence of chaotic spiking and bursting activity with a long period in the parameter space of the reduced model. This co-existence is shown in Figure 3.6. 2) The transition from the bursting activity into silence is associated with the homoclinic bifurcation for unstable periodic orbit. The co-existence of bursting activity and silence is found, see Figure 3.7. This co-existence is due to the unstable periodic orbit, whose stable manifold separates the basin of attraction of the bursting and silent attractors. In the parameter plane, the

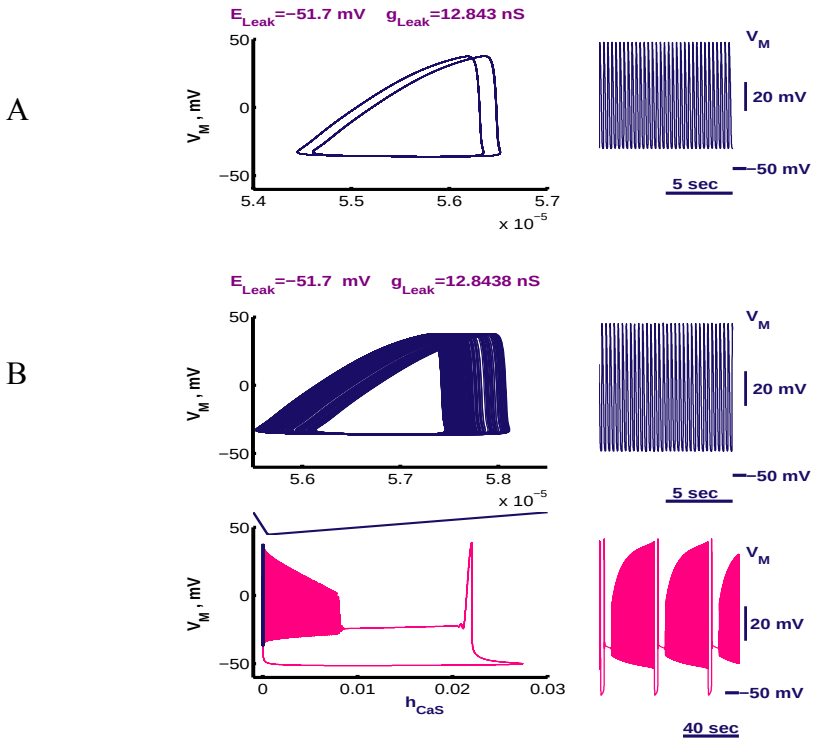

Figure 3.6. Period doubling cascade and the coexistence of chaotic spiking and bursting activity in the reduced model. A) Here the transition between tonic spiking and bursting activities occurs through period doubling cascade. The right column of the figure yields the corresponding voltage traces. B) The coexistence of the bursting activity and chaotic tonic spiking takes place at E_{leak}=-51.7 mV, g_{leak}=12.3638 nS.

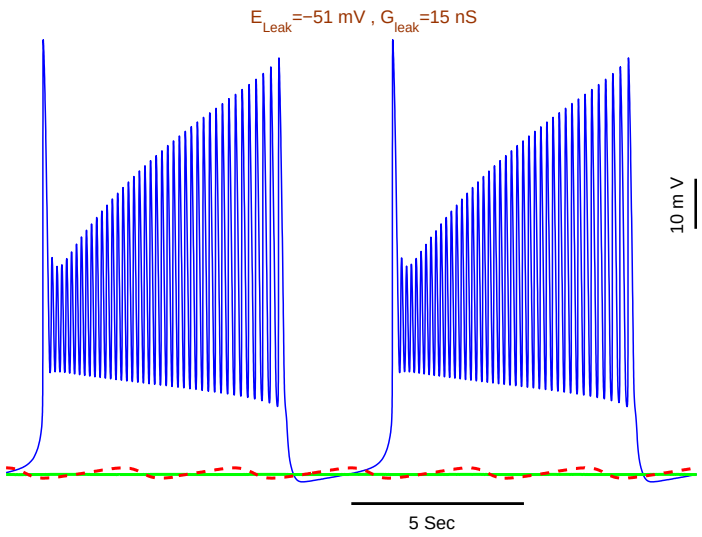

Figure 3.7. Coexistence of two attractors for the simplified model is shown. The bursting activity (blue) and the silence (green) are separated by the unstable periodic orbit (red) at E_{leak}=-51 mV, g_{leak}=15 nS.

coexistence region is bounded by the homoclinic and subcritical Andronov-Hopf bifurcation curves. This region is marked as the co-existence in Diagram 1.

For the model with the canonical parameter values, we have studied the (g_{leak},E_{leak}) - parameter bifurcation diagram (see Diagram 1). It shows the relative position of two homoclinic bifurcation curves and two Andronov-Hopf bifurcation curves. Between the corresponding bifurcation curves the periodic orbit exists in the model: it terminates at the homoclinic bifurcation and begins through Andronov-Hopf bifurcation. The shaded area between the two homoclinic curves is the domain of the bursting activity (green in Diagram 1). We have found that bursting activity and the silent regime are separated by unstable sub-threshold oscillations. The switch between two activities can be performed by a pulse of current. Figure 3.8-3.9 show the series of numerical experiments where silence and the bursting regimes are perturbed by a pulse of hyperpolarizing current. The hyperpolarized current leads to the switch of activity from bursting into silence as soon as the pulse of current passes the phase point of the trajectory inside

the unstable periodic orbit (marked by the red points in Figure 3.8 (A)). As long as the phase point travels outside of the unstable periodic orbit (see Figure 3.8 (B)), the neuron remains in the bursting regime. Figure 3.9 demonstrates the perturbation of silence into bursting. Similarly, if the perturbation with a pulse of injected current moves the phase point away from the

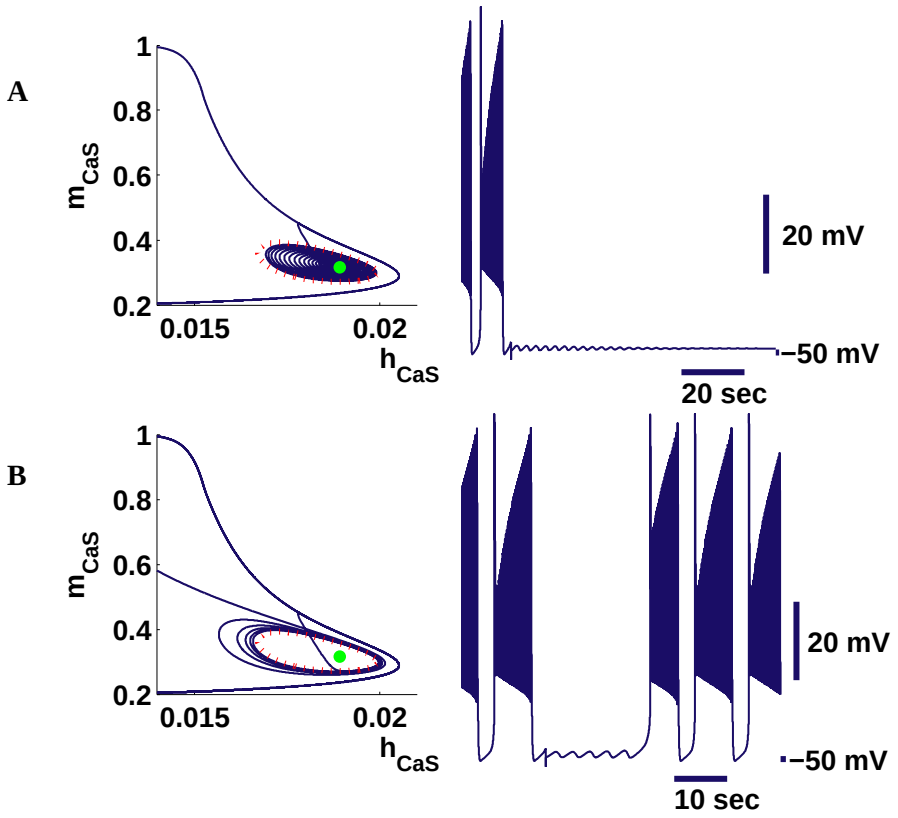

Figure 3.8. Perturbations of bursting activity by a pulse of current for the simplified model (I_{Na}, I_{CaS}). Parameters of the model have values g_{leak}=15 nS, E_{leak}=-0.051 V, Bh=0.031 V, the duration of the pulses are 0.01 sec. On the left side of the figure in the (m_{CaS}, h_{CaS}) plane, the phase trajectory of the activity before and after injection of the pulse is plotted. The green dot is the stable equilibrium point. The red dotted curve marks the unstable periodic orbit. On the right side of the figure, the voltage traces are shown. A) The hyperpolarized pulse of the current with amplitude -0.264 nA switches the activity from bursting into silence. The phase point of the trajectory is moved inside the unstable periodic orbit, and the bursting activity is not the attractor anymore. B) The hyperpolarized pulse of current is injected when the neuron shows bursting activity. It does not produce a switch between the activities. The pulse of the current brings the phase point close to the unstable periodic orbit, but the phase point is outside of the periodic orbit. The amplitude of the pulse is -0.26 nA.

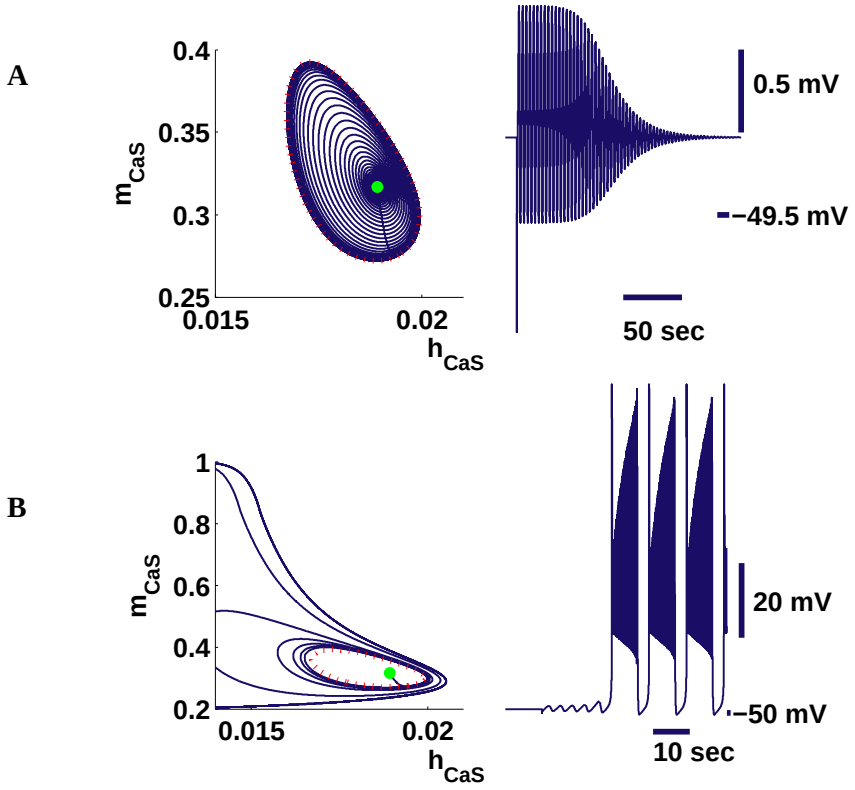

Figure 3.9: Perturbation of silent regime for the simplified model (I_{Na}, I_{CaS}). Parameters of the model have values g_{leak}=15 nS, E_{leak}=-0.051 V, Bh=0.031 V, the duration of the pulses are 0.01 sec. The hyperpolarized pulse of the current perturbs the silent mode. The silent mode (stable equilibrium) is shown by the green dot. A) The hyperpolarizing pulse of current with amplitude -0.0677 nA moves the phase point toward the unstable periodic orbit, but the pulse is not strong enough to put the phase point outside of the unstable periodic orbit. B) The hyperpolarized pulse of current with amplitude -0.07 nA switches the activity from silence into bursting. The phase point of the trajectory is moved outside of the unstable periodic orbit and silence is not the observed regime anymore.

equilibrium state, outside of the unstable periodic orbit (see Figure 3.9 (B)), the system will switch from bursting activity into silent one. Otherwise, as Figure 3.9 (A) demonstrates, the neuron produces damping oscillations and returns to the silent regime.

Next, let us to show the similarity in the dynamical behavior of the simplified model and of the complete model. First, we would like to pose the following questions: is the mechanism of the co-existence maintained in the complete model? Will similar stimulation procedures reveal

the bi-stability in the complete model? We will answer and discuss the answers to these questions in the next chapter.

Canonical model of a leech heart interneuron

In this section we study the canonical model of the leech heartbeat neuron. This biophysically accurate model (Hill et al., 2001) following Hodgkin-Huxley's formalism (Huxley, 2002) is based on the dynamics of the eight distinct voltage dependent currents: five inward and three outward and a passive leak current which is not voltage dependent. The model was tuned to reproduce the characteristics of the neuron's activity such as the period of bursting activity, burst duration and the frequency of the spikes in a burst observed experimentally.

The analysis is based on the systematic variation of E_{leak} and g_{leak} to explain the difference in experimental data obtained by two different techniques of recording of neuronal activity: intracellular and extracellular. During the intracellular method, a neuron is penetrated by a sharp glass electrode. It allows the membrane potential to be directly recorded. The main advantage of this method is that current can be injected into the cell; therefore one can control the membrane potential of the cell. The downside of the technique is that the cell gets damaged. During the extracellular recording a cell is sucked inside of the glass electrode and the membrane potential can be measured directly. We can not control the activity of the cell by this method, but it is not as harmful as the intracellular method. Cymbalyuk et. al 2002 showed that the activity of the leech heart neuron is highly sensitive to the method of recording. Intracellular recording of the single heart neuron in bicuculline (bicuculline blocks the synaptic connections of neurons) shows tonic spiking activity; however during extracellular recording the neuron endogenously

produces bursting activity. It has been proposed then that intracellular recording generates an additional leak current. This shunting component of the leak current can suppress the endogenous bursting activity (Cymbalyuk et al., 2002).

The analysis of the model of the cell has shown that changes in the leak current cause the transitions between different behaviors of the neuron. For instance, increase of conductance of the leak current switches the neuron from tonic spiking into bursting activity (Cymbalyuk et al, 2002). The bifurcation analysis of the neuron model allows us to elucidate the role of the currents in the regulation and control of these activities. Here we focus on the complex dynamics supporting the co-existence of two different regimes, bursting and silence. Because the activity of the neuron model is sensitive to the leak current, we construct the bifurcation diagram in the leak current ($g_{leak,}$ E_{leak})-parameters plane. The diagram demonstrates the borders between different activities (bursting and silence), and the area of their co-existence. The areas of tonic spiking, bursting activity, silence and multistability were determined in Cymbalyuk et. al. 2002 (see Diagram 2). The area of co-existence was shown to be bounded by the curve corresponding to the Andronov-Hopf bifurcation; however the boundary near which the bursting activity disappears was not determined analytically, and the exact mechanism of the transition was left beyond the scopes of the paper.

Switching the activities between silence and bursting by a pulse of current

To examine the behavior of the neuron in the bi-stability regime, we choose the g_{leak} and E_{leak} parameters from bifurcation Diagram 2, where the neuron model shows the co-existence of silence and bursting. For the parameters g_{leak}=9.86 nS and E_{leak}=-0.065 V both types of activities exist and can be chosen depending on the initial state of the model. First, we explore the reaction

of the neuron at the silent regime (see Series 1 in Figure 3.10). A depolarizing pulse of current with duration of 0.1 sec and amplitude -0.05 nA is applied to the model. This pulse depolarizes

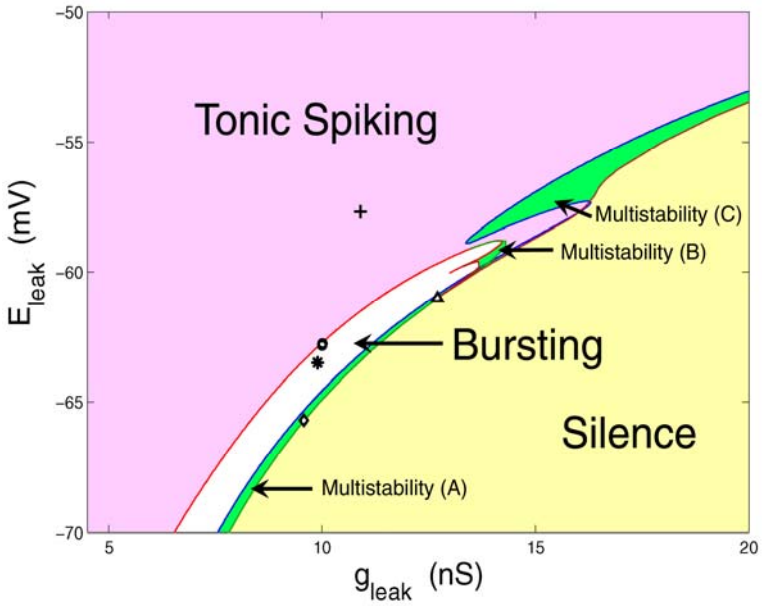

Diagram 2: Bifurcation diagram of the canonical 14 D leech heart interneuron model. The pink, orange, and yellow areas mark the parameter regimes where tonic spiking, bursting, and silence are stable, respectively. Green and blue areas mark regions of multistability. Multistability (A) points to the area (marked blue) where bursting coexists with silence; multistability (B) points to the area where bursting co-exists with tonic spiking; multistability (C) points to the area where tonic spiking co-exists with silence.(The diagram is taken from Cymbalyuk et al, 2002)

the model and leads it to the transition from silence into bursting (Numerical Experiment 1 from Series 1). This observation determines a threshold, which separates the activities. On the other hand, when we apply a hyperpolarizing pulse of current with an amplitude of 0.05 nA and duration 0.1 sec, the injected current hyperpolarizes the silent regime of the model. Intuitively, the neuron model should stay in silent regime when the neuron is hyperpolarized. Numerical Experiment 2 from Series 1 (see Figure 3.10) shows the activity of the model (when hyperpolarized current is injected) is

Series 1: Perturbation of silent regime into bursting activity.

Numerical Experiment 1.

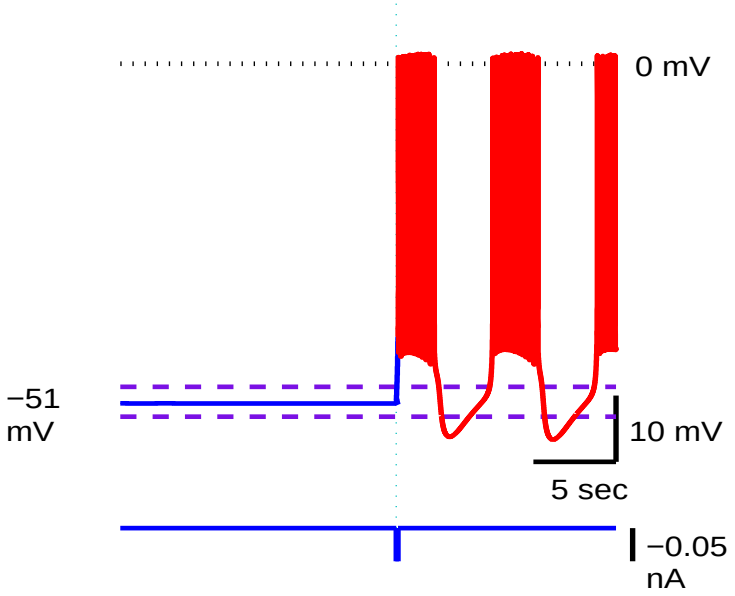

Numerical Experiment 2.

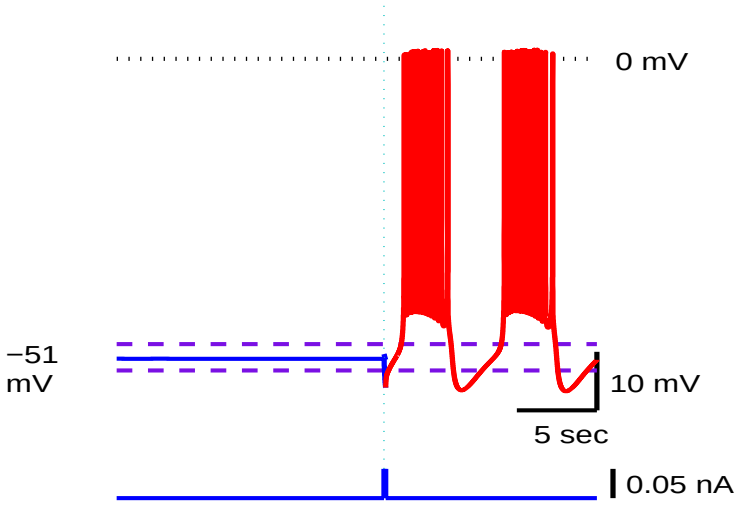

Figure 3.10: Duration of the pulse is 0.1 sec. The parameters of the model are g_{leak}=9.86 nS E_{leak} =-0.065 V. The purple dashed lines indicate the maximum and minimum values of amplitude of the unstable sub-threshold oscillations. Experiment 1. Perturbation of the system by the depolarizing pulse of current is plotted Amplitude of the pulse is -0.05 nA, it depolarizes the cell and causes the transition from silence to bursting. Experiment 2. Perturbation of the system by the hyperpolarizing pulse of current is plotted Amplitude of the pulse is 0.05 nA, it hyperpolarized the cell and also causes the transition from silence to bursting.

counterintuitive. Either, a hyperpolarizing or a depolarizing pulses of current lead to the onset of bursting activity. The series 2 of our numerical experiments are performed on the model which initially exhibits bursting activity (see Series 2 in Figure 3.11). We inject a hyperpolarizing pulse of the current with the purpose of pushing the system into a silent regime. As shown in Numerical Experiment 3, a hyperpolarizing pulse of the current with amplitude 0.1 nA and duration 0.1 sec perturbs the system so that the phase point leaves the bursting attractor and moves into the silence mode. Then the hyperpolarized pulse of current is increased until the amplitude of the pulse reaches 0.4 nA. Instead of hyperpolarized silence which was expected, the neuron model produces bursting activity (see Numerical Experiment 4 of Series 2).

The traditional view of neuronal activity suggests that the increase of the hyperpolarizing pulse of the current has to lead to the hyperpolarized silence. However, this does not account for the co-existence of silence and bursting, as in our case. Our numerical experiments imply two thresholds: upper and lower. The presence of unstable sub-threshold oscillations can explain the existence of the two thresholds.

Life and death of sub-threshold oscillations

To explain the results of numerical experiments with the perturbations, described in the previous paragraph, we perform the bifurcation analysis of the stationary and oscillatory states of the model. First, we use g_{leak} and E_{leak} parameters and set them so that the model has only one attractor, a stable hyperpolarized stationary state (silence). Then, we will analyze the stability of the stationary state as g_{leak} is varied.

Series 2: Perturbation of bursting activity into silent regime

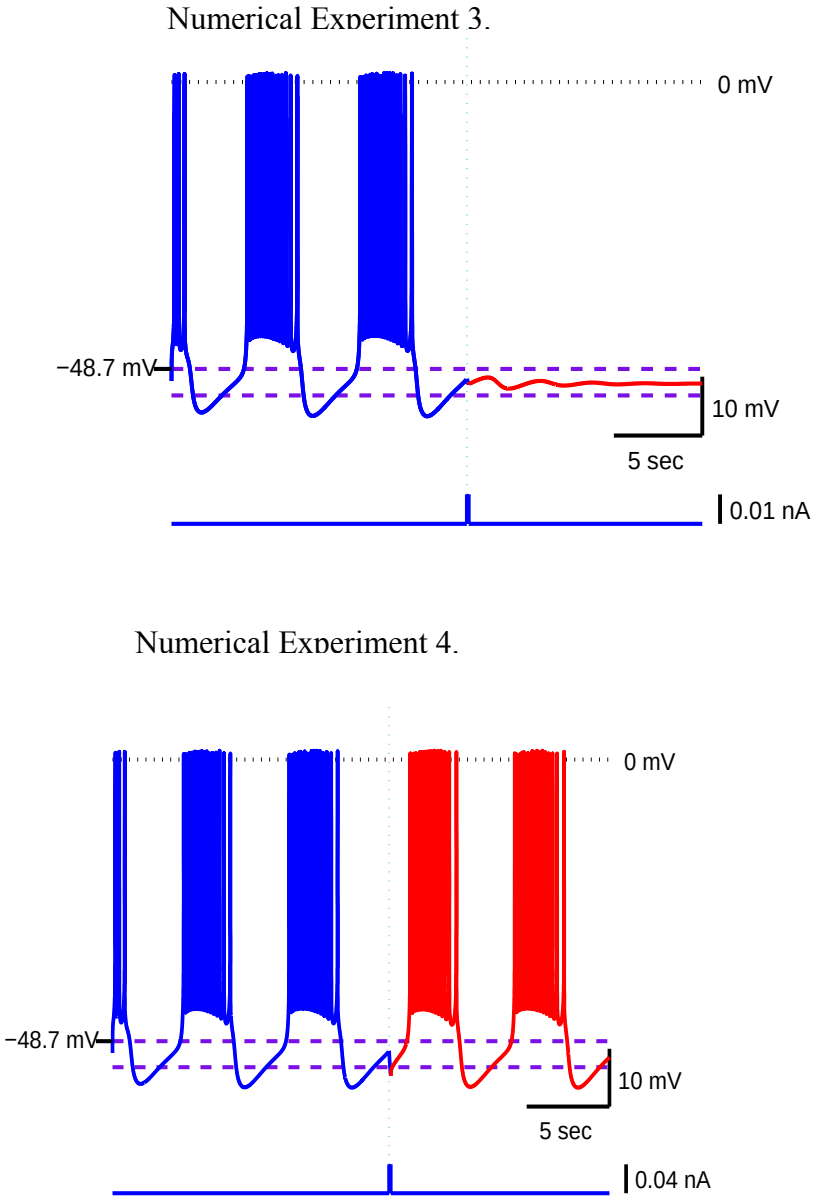

Figure 3.11: Duration of the pulse is 0.1 sec. The parameters of the model do not change: g_{leak}=9.86 nS E_{leak} =-0.065 V. The purple dashed lines indicate the maximum and minimum value amplitude of the unstable sub-threshold oscillations. Experiment 3 shows the co-existence of the bursting activity and silence regimes. Perturbation of the bursting leading to silence via the hyperpolarizing pulse of current is shown. Pulse's amplitude is 0.01 nA. Experiment 4 shows the case where perturbation does not change the regime of the cell. Perturbation by a hyperpolarizing pulse of the current is shown. The amplitude of the pulse is 0.04 nA. The pulse hyperpolarizes the cell and does not switch the activity from bursting into silence.

The stability of the stationary state is evaluated through the characteristic exponent or the eigenvalues of the Jacobian. If all the eigenvalues have negative real parts, then the stationary state of the system is stable. The calculation of the eigenvalues is performed using Content (Kuznetsov et al.,1996). At the parameters g_{leak}=33 nS and E_{leak}=-0.058 V the model displays only the hyperpolarized silent regime. By varying the parameters, we find the curve of the equilibrium. It has a stable branch (green curve in Figure 3.12) composed of stable equilibrium states, and the unstable branch composed of the equilibrium states of the saddle and saddle-focus type, which is shown as the blue dashed curve in Figure 3.12. At the critical value g_{leak}^{0}=15.71 nS, the equilibrium state undergoes subcritical Andronov-Hopf bifurcations. This leads to the onset of unstable sub-threshold oscillations. Near the bifurcation, the increase of the amplitude of the unstable periodic orbit is evaluated as $\sqrt{g_{leak} - 15.71}$ (see Figure 3.13). At the bifurcation, the frequency, ω, of a periodic orbit is given by the imaginary part of the two eigenvalues, and in the vicinity of the bifurcation the period is $T \approx 2\pi/\omega + O(g_{leak} - g_{leak}^{o})$. After the Andronov-Hopf bifurcation, the geometry of the periodic orbit becomes distorted as g_{leak} changes from the bifurcation parameter g_{leak}^{0}. For example, the integration of the solutions of the system for parameters g_{leak}=15.71 nS and E_{leak}=-0.058 V gives the frequency of the oscillations ω=1.95 rad/sec, therefore the period of the new born cycle is 3.22 sec. For g_{leak} smaller than 15.71 nS the real parts of the two eigenvalus are positive, and the equilibrium state becomes a saddle-focus.

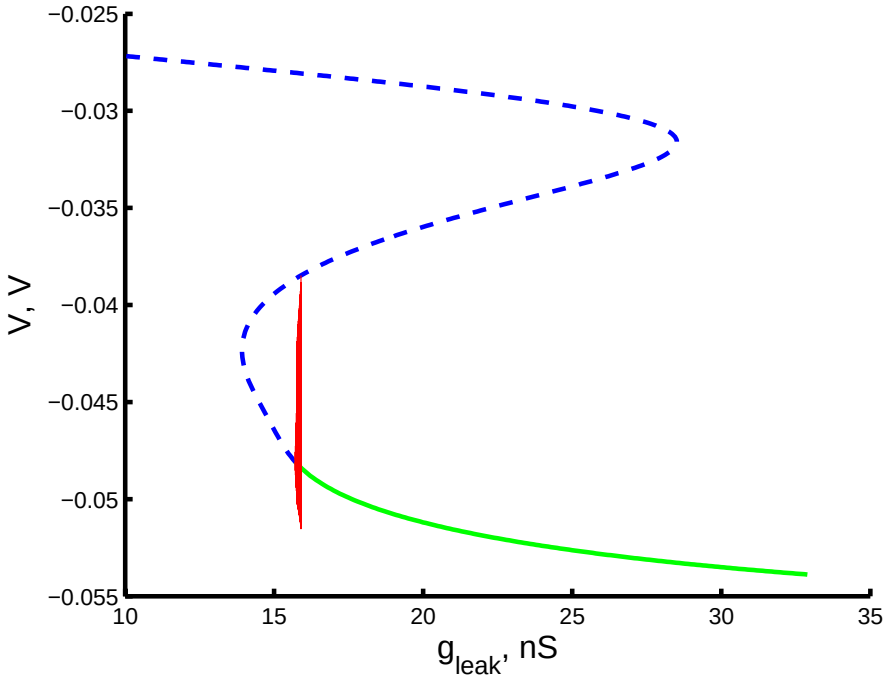

Figure 3.12: Rapid growth of the unstable periodic orbit (red) toward the curve of the equilibrium. The periodic orbit emerges through the Andronov-Hopf bifurcation at g_{leak}=15.71 nS and E_{leak}=-0.058 V and ends up at the homoclinic bifurcation. The increase of g_{leak} leads to the increase of the amplitude and the period of the periodic orbit. The stable branch of the equilibrium is marked by the green curve. The unstable branch of the equilibrium is represented by the blue dashed line.

The further increase of the parameter g_{leak} leads to the increase of the amplitude and the period of the unstable periodic orbit; the periodic orbit swells (see Figure 3.12 and Figure 3.13). The evolution of the unstable periodic orbit relative to the curve of the equilibrium is presented in Figure 3.12. As the parameter reaches the value g_{leak}=15.7522 nS, a saddle-node bifurcation of the periodic orbits occurs. As Figure 3.13 shows, the unstable periodic orbit collides with the stable periodic orbit and both are annihilated. At the figure, orbits are shown by the solid and dashed lines, respectively. The secondary saddle-node bifurcation of the periodic orbit occurs at the parameter g_{leak}=15.7542 nS. At this bifurcation, the stable and unstable periodic orbits meet

and merge. Two vertical lines in Figure 3.13 indicate the small region where the three stable regimes can co-exist: bursting, silence and stable sub-threshold oscillations.

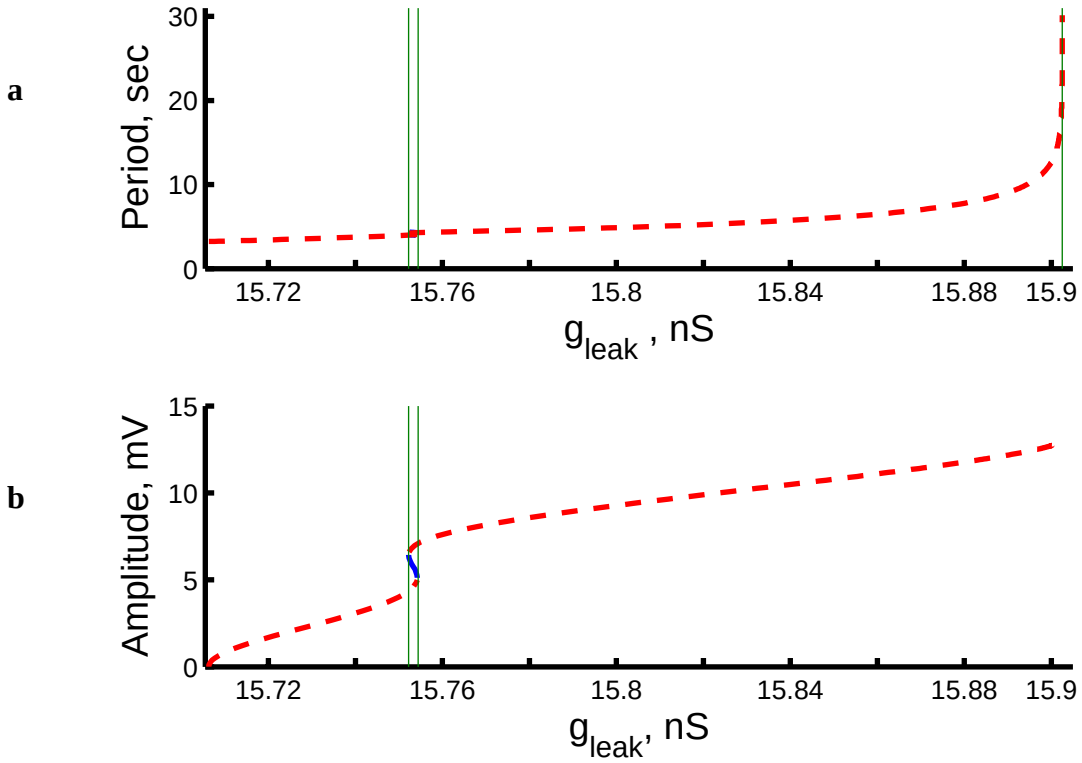

Figure 3.13: Dependence of the period and amplitude on g_{leak}. a) The relatively small change in the parameter g_{leak} near the homoclinic bifurcation leads to the rapid increase of the period of the periodic orbit. It is presented by the green line at g_{leak}=15.905 nS. b) The change of the amplitude of the periodic orbit, when g_{leak} is in the region of 15.9 nS, is small. At gleak=15.7522 nS and 15.7542 nS the saddle-node bifurcations for a periodic orbit occurs. The green line corresponding to g_{leak} ={15.7522 15.7542} nS indicates the region where stable periodic orbit exists.

Figure 3.14 shows that for $g_{leak} > g^{o}_{leak}$ there are two attractors in the model which are a stable stationary state (the green line) and bursting attractor (the blue curve). These two attractors are bounded from each other by the unstable periodic orbit (the red dashed curve). Now we can explain the meaning of the upper and lower threshold. This unstable periodic orbit determines the basin of attraction of both attractors. Inside it, the phase point converges to the stationary state. Outside of this saddle periodic orbit, it is attracted to the bursting activity. The minimal

and maximal values of the voltage of the unstable periodic orbit define the two thresholds. As shown in Figures 3.10-3.11 (Series 1 and 2), the dashed lines indicate the max and min value for the amplitude of the unstable sub-threshold oscillations.

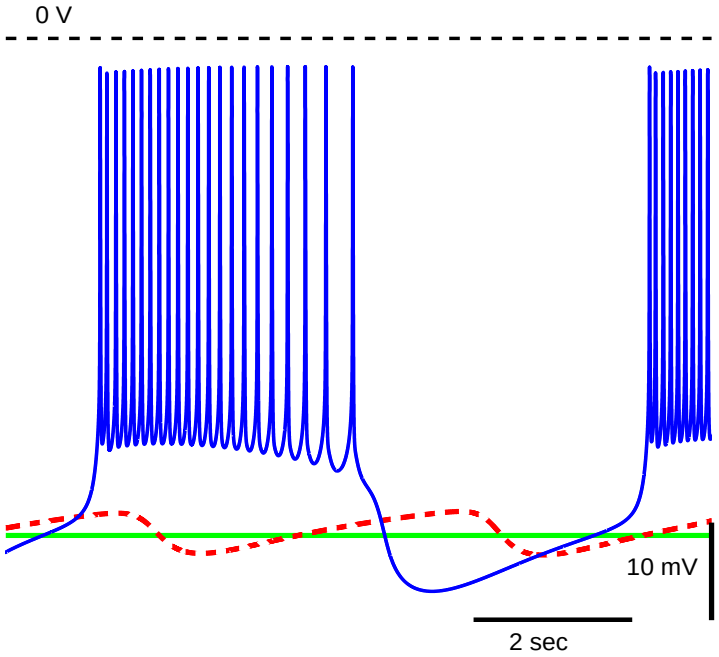

Figure 3.14: Coexistence of the silence and bursting activities separated by unstable subthreshold oscillations for the complete model. The green line marks the stationary state (silence) of the model, the blue curve represents bursting activity, the red dashed curve marks unstable sub-threshold oscillations. Sub-threshold oscillations define the basin of attraction. Inside of the unstable periodic orbit only the silent mode can exist. Across of this orbit bursting activity is the stable regime. Minimum and maximum values of the amplitude of the unstable periodic orbit define two thresholds: upper and lower. g_{leak} and E_{leak} are 9.86 nS and -65 mV

Now, let us explain the experiments with perturbations by the current. If the pulse of the current is sufficiently large to move the phase point from the stationary state away through the threshold, the neuron goes into bursting activity (see Numerical Experiments 1-2 in Figure 3.10). The switching pulse of the injected current can be either hyperpolarized or depolarized. In the second series of numerical experiments, the neuron initially shows the bursting activity. The pulse of the current has the amplitude in approaching phase, which puts the phase point inside of the unstable periodic orbit. When current is injected, the neuron switches into the silent regime

(see Numerical Experiment 3). If the pulse amplitude is too large, and the neuron is hyperpolarized below the minimum voltage of the unstable sub-threshold oscillations, the phase point will remain in bursting activity regime (see Numerical Experiment 4). The transition from bursting into silence is easy to initiate when the pulse is injected at specific moments. The voltage coordinate of the phase point of the bursting activity has to be close to the voltage of the silent regime. For example, for E_{leak}=-0.058 V and g_{leak}=15.9 nS, the basin of attraction is defined by two thresholds with V_{min}= -51.52 mV and V_{max}= -38.48 mV. Figure 3.14 shows the co-existence of the stable equilibrium and the bursting activity separated by the unstable sub-threshold oscillations.

The period of the unstable periodic orbit changed rapidly from 6 sec to 30 sec as g_{leak} is increased from 15.87 nS to 15.9 nS, (see Figure 3.13 a). This indicates indirectly that a homoclinic bifurcation is about to occur in the system. As the periodic orbit comes close to the saddle, its period increases proportionally to $\ln(\frac{1}{g_{leak} - g^*_{leak}})$. At the same time (Figure 3.13 b) the amplitude of the oscillations stays relatively constant O(1). As g_{leak} increases toward the critical value, g^*_{leak}, the unstable periodic orbit bands into the saddle point (see figure 3.12), creating a homoclinic loop, and vanishes. Once g_{leak} passes the critical value g^*_{leak}, the saddle connection breaks up and the homoclinic loop is destroyed.

With the help of the software Content, this bifurcation can be detected numerically. The feature of this bifurcation is that as the periodic orbit approaches the critical value, the period grows logarithmically. The evolution of the unstable periodic orbit relative to the location of the equilibrium states, as g_{leak} is varied, is presented in Figure 3.15. At the figure, the green dots

represent the projection of the stable equilibrium for a given $g_{leak,}$ on to the m_{CaS} and h_{CaS} plane, and the red points correspond to the saddle equilibrium states.

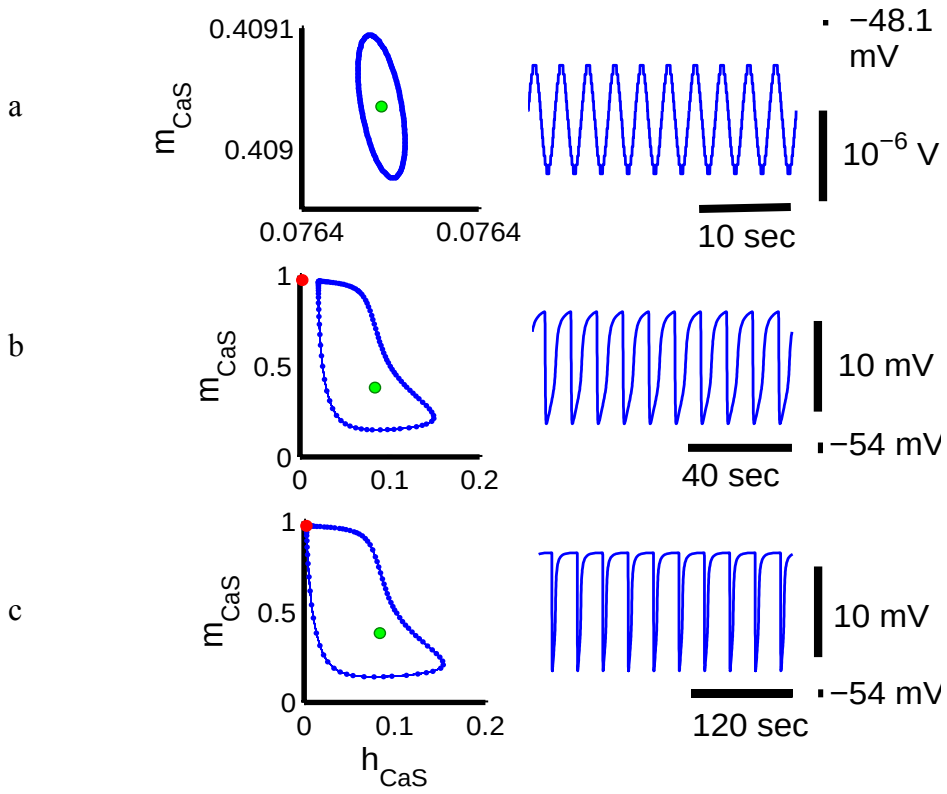

Figure 3.15: Evolution of the unstable periodic orbit in the (m_{CaS}, h_{CaS}) plane and corresponding traces (V v.s t), as parameter g_{leak} is varied. For this set of numerical experiments E_{leak} is -0.058 V. a) The unstable periodic orbit is born through sub-critical Andronov-Hopf bifurcation. Parameter value is g_{leak}=15.71 nS, producing the oscillations with Period=3.23 sec. Amplitude of the oscillations is small and equal to 1.2 μV. b) The parameter g_{leak} is increased to 15.89 nS, period and the amplitude increase, Period=10 sec and Amplitude=12.4 mV. c) Now, as the parameter g_{leak} barely changes to g_{leak}=15.9 nS, the period increases quickly, Period =30 sec while the amplitude almost does not change Amplitude=13 mV.

When the parameter g_{leak} increases, (Figure 3.15) the periodic orbit expands toward the saddle point. As the periodic orbit gets closer to the saddle point, the phase point spends more time in the vicinity of this point; therefore the period drastically increases (Figure 3.15 c)). At the moment when the trajectory of the periodic orbit passes through the saddle point, the homoclinic bifurcation occurs. The unstable periodic orbit disappears and now the stationary state is the only

attractor. The trajectory of the bursting activity after the homoclinic bifurcation can not be observed anymore. With these critical parameters, if the initial conditions are chosen so that the neuron is showing transient bursting activity, the number of bursts before the neuron settles down at the rest potential is not predictable (Figure 3.16). At this bifurcation, the transition from bursting into silence is defined. It shows that near the border which is defined through the homoclinic bifurcation the model exhibits the phenomenon of intermittent transition from bursting into silence.

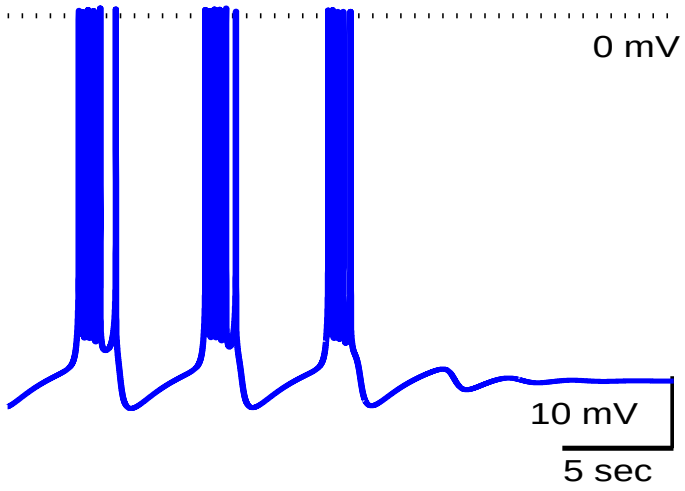

Figure 3.16: Intermittent transition from bursting into silence for the complete model.

We determine a pair of parameter values of g_{leak} and E_{leak} for which the unstable periodic orbit has period 30 sec. On time scale of the processes in the model, this is considered very long and therefore close to the homoclinic bifurcation parameters. To find the periodic orbits with a certain period, we introduce a function $F(T_o, T(g_{leak}, E_{leak}))$, where

$F(T_0, T(g_{leak}, E_{leak})) = T(g_{leak}, E_{leak}) - T_o$, $T(g_{leak}, E_{leak})$ is the period of the unstable periodic orbit, T_o = 30 sec. Content can detect and continue the zero of this defined function in the two-parameter space. This lets us determine $F(T_0, T(g_{leak}, E_{leak})) = 0$ and find the pair of values (g_{leak} , E_{leak}) comprising the isochrone of the given period. This method allows for the finding of the set of periodic orbits of given period. We constructed the (g_{leak}, E_{leak})-parameter bifurcation diagram, where the transition between bursting activity into silent mode and one of the borders of the co-existence have been defined through the homoclinic bifurcation. As Diagram 3 shows, one of the borders of the area of co-existence of bursting activity and silence, that was introduced in Cymbalyuk et al., 2002, matches closely with the predicted value for the homoclinic bifurcation points.

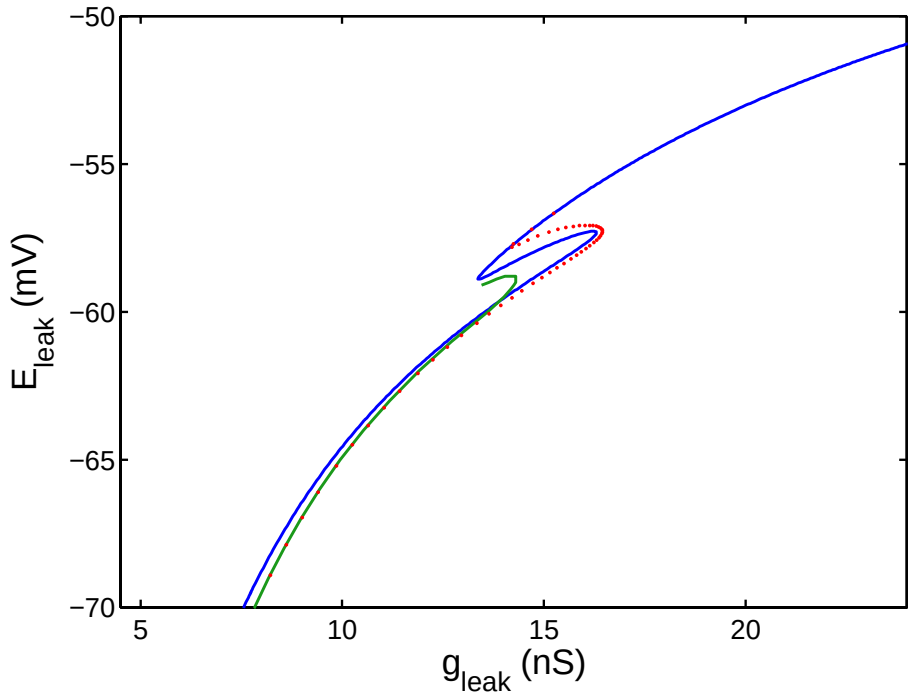

Diagram 3: Area of the co-existence of bursting activity and silence is defined by the subcritical Andronov-Hopf and homoclinic bifurcation curves. The blue curve corresponds to the Andronov-Hopf bifurcation. The green curve shows the border where the transition from bursting into silent regimes occurs (Cymbalyuk, G.S., et al., 2002). The red dots mark the points where the homoclinic bifurcation occurs.

We have shown that the unstable hyperpolarized sub-threshold oscillations (periodic orbit) emerge through the Andronov-Hopf bifurcation and disappear through the homoclinic bifurcation. Diagram 3 shows the Andronov-Hopf bifurcation curve on which the second border of the area of the co-existence is defined.

In conclusion, we showed that the unstable sub-threshold oscillations separate the stable equilibrium (rest state) and bursting activity. Minimum and maximum values of the voltage of the unstable periodic orbit define two thresholds: upper and lower. It explained the series of numerical experiments where the switch between different regimes can be produced by a pulse of current of certain amplitude. We showed the area of co-existence of bursting activity and silence is defined by the sub-critical Andronov-Hopf bifurcation and a homoclinic bifurcation. The homoclinic bifurcation explains the transition from bursting into silence.

DISCUSSION

Basic patterns of neuronal activities are silence, sub-threshold oscillations, tonic spiking and bursting activity. A number of theoretical and experimental studies have demonstrated that both a single neuron and neuronal populations can exhibit bi-stability, in other words, these regimes can co-exist with one another (Wang et al., 1995; Shilnikov et al., 2004; Milton and Jung, 2003; Cymbalyuk et al., 2002; Cymbalyuk et al., 2000; Feoden and Grebogi, 1997; Gadatela and Dangelmayr, 2001; Manning et al., 2003; Manuca et al., 1998).

In cortical neurons, many classes display transitions between tonic spiking and bursting as a function of the brain state, for example sleep versus wakefulness (Steriade, 2001). The co-existence of tonic firing and bursting has been shown in cortical neurons (Fröhlich. and Bazhenov, 2006). Depolarization of a neuron caused by raised extracellular K^+ concentration can lead to bursting in a cell which usually shows tonic spiking. (Jensen et al., 1997). The increase of K^+ concentration during epileptogenesis is an established fact (Somjen et al., 2004; DeLorenzo et al., 2005). Frohlich and Bazhenov developed a cortical neuron model which explains bi-stability between tonic spiking and bursting for raised K^+ concentration. The leech heart interneuron model also exhibits co-existence of two types of oscillations: tonic spiking and bursting with large amplitude (Shilnikov et al., 2004). Switching between these two regimes can be produced by modulation of the initial state of the neuron model (Shilnikov et al., 2004). Bursting is separated from tonic spiking by an unstable periodic tonic spiking activity of the saddle type, which determines the threshold between regimes.

Here, we investigated a mechanism of bi-stability of the model of the leech heart interneuron. We have illustrated its properties by a series of numerical experiments. They display

that the activity of the cell which was initially in the silent regime can be switched into bursting activity by depolarized and hyperpolarized pulses of the current. In the other series of experiments, where the neuron was initially in the bursting mode, we showed that it can be switched into the silent mode by a hyperpolarized pulse. In the later case, if the amplitude of the hyperpolarized pulse is increased, the cell returns to bursting activity. These numerical experiments imply two thresholds: upper and lower. We have shown that switching between bursting activity and silence can be controlled by a pulse of current.

The knowledge of the mechanism of bi-stability is useful in the design of treatments of such medical conditions as Parkinson's disease, sudden infant death syndrome (SIDS), epilepsy, and essential tremor (Breakspear et al., 2006; Harvey et al., 2007; Milton and Jung, 2003; Wang et al., 1995; DeLorenzo, 2005; Weese-Mayer et al., 2007). What is common for these medical conditions is that they are examples of *dynamically* dysfunctional activities of neuronal system (Feudel et al., 1997; Gadaleta et al., 2001; Manning et al., 2003; Milton and Jung, 2003). For example, SIDS is defined as a sudden, unexpected death of an apparently healthy infant under one year of age, usually during sleep (Weese-Mayer et al., 2007). It has been suggested that this syndrome could be a result of the bi-stability of the neuronal system, where death is associated with the silent regime.

Damage of the neurons might cause a change in the activity of the whole neural network and lead to epilepsy (DeLorenzo et al., 2005; Milton and Jung, 2003). Epilepsy can be generated in a large group of cells. It is the most common serious condition in neurology. Seizures are frequently accompanied with synchronized hyperactivity in the neuronal network and the cells are depolarized to a high level (Drongelen et al., 2003). A weak electrical field can modulate neuronal activity (Francis et al., 2003). It has been shown that deep brain stimulation can provide

noticeable benefits for people with tremor or Parkinson's disease. High frequency stimulation of the intermediate nucleus of the thalamus essentially could relieve tremors (Perlmutter et al., 2006). There are a number of experiments in which the seizure can be stopped by a pulse of current (Milton and Jung, 2003; Perlmutter et al., 2006).

Exemplary ideas of bi-stability are exploited in designs of treatment of Parkinson's disease. Under normal conditions, particular neuronal populations located in the thalamus and the basal ganglia show apparently random electrical activity, whereas abnormal synchronized activity of these neurons is associated with Parkinson's resting tremors (Alberts et al., 1969). The main question is how to suppress that abnormal synchronized activity. Tass and Hauptmann created a model of the subthalamic nucleus (STN) (Tass and Hauptmann, 2007). Its analysis shows that appropriate electrical stimulation of the bursting neurons located in the thalamus may change synaptic wiring of the neuronal networks. It gives rise to the co-existence of different dynamically stable regimes. Due to this multistability of the neuronal network, it is possible to switch the network activity from the strongly synchronized state to a desynchronized state. It has been proposed that suppression of synchronized activity is based on two plasticity induced effects. The first is desynchronizing stimulation, which causes a decrease of synaptical weights. The second effect requires that the weakly synchronized state must be stable (Tass, 2001). To solve the problem of abnormal synchronization, authors have suggested applying weak or short stimulation. This stimulation causes a reduction of a pathologically synchronized neuronal population (Tass, 2001; Tass and Hauptmann, 2007). The main advantage of such stimulation, that it does not affect memory as much as alternative methods which are based upon longer stimulation. To induce the switch from abnormal to normal neuronal activity, Tass suggests using a two pulses deep brain stimulation techniques.

Discussing treatment of epileptic seizures, Milton brought into consideration the co-existence of two patterns of tonic spiking activities that arise in membrane potential of an *Aplisia* motoneuron. When the single stimulation is applied the switch between activities occurs (Milton and Jung, 2003). Designing methods of feedback stimulation, Milton shows that multistability can appear in the models of delayed feedback control. The necessary conditions for multistability were established as following; the sum of the conduction times along the axon and dendrites, time required for quantal release, processing times in the neurons, and the rise time of synaptic inhibition has to be greater than the intrinsic firing period of the neuron. Multistability was presented as the multiple basins of attraction separated by ridges of varying heights that correspond to energy barriers (Milton and Jung, 2003). Such a dynamical system can be controlled and manipulated with small perturbation. Milton has designed a feedback stimulation method of regulation of neuronal network activity. At each moment of time when the abnormal attractor occurs, the feedback stimulation imposes the initial conditions for the normal attractor (Milton and Jung, 2003).

In 2002, Netoff and Schiff have proposed that a decrease in synchronization is essential for initiation and maintenance of epileptic seizures. If synchrony is associated with seizure termination, then the method directed at increasing such synchronization may be useful in controlling seizures (Netoff and Schiff, 2002).

Our results explain a novel mechanism bi-stability at the cellular level. If neurons in a population where each neuron possess the property of bi-stability of bursting and silence according to the mechanism described here, then we can provide specific instructions for the design of electrical stimulation. According to the scenario described, two attractors are separated by the unstable periodic orbit, which was born through Andronov-Hopf bifurcation. The

perturbation by the pulse of current can be applied to the group of cells. If the pulse of current is injected with appropriate amplitude and at the specific phase, the bursting can be locked into the silent regime. The theory of bi-stability and the controlling mechanism might be applied to the design of a treatment of tissue displaying epileptic behavior. The feedback techniques may suppress the abnormal activity of the neuron by switching into the normal regime.

In conclusion, we described a novel mechanism explaining the co-existence of bursting and silent regimes in a single neuron. We demonstrated how the injection current pulse can be applied with the certain amplitude and at the specific phase to make a switch between regimes. We demonstrated that the specific characteristics of the pulse are defined by the unstable sub-threshold oscillations which separate two basins of attraction (bursting and silence). The mechanism of supporting the co-existence is similar for both the simplified four dimensional model and the complete fourteen dimensional model. In both models the area of co-existence is determined by two bifurcations: Homoclinic and Andronov-Hopf. The hypothesis is that the area of the co-existence of bursting and silence is defined by two types of bifurcations, which might give a general principal for controlling bi-stability in a Hodgkin-Huxley type model.

REFERENCES

1. Alberts W. W., Wright E. J., Feinstein B., *Cortical potentials and parkinsonian tremor.* Nature, 1969. **221**: p. 670–672.
2. Angstadt J. D., *Persistent inward currents in cultured Retzius cells of the medicinal leech.* Journal of Comparative Physiology A: Neuroethology, Sensory, Neural, and Behavioral Physiology, 1999. **184**(1): p. 49-61.
3. Arbas E.A. and Calabrese R.L., *Leydig neuron activity modulates heartbeat in the medicinal leech.* J Comp Physiol 1990. **167**: p. 665–671.
4. Arbas E. A., Calabrese R. L., *Rate modification in the heartbeat central pattern generator of the medicinal leech.* J Comp Physiol 1984. **155:** p. 749–761
5. Arshavsky Y. I., Deliagina T. G., Orlovsky G. N., Panchin Y. V., Pavlova G. A., Popova L. B., *Control of locomotion in marine mollusc Clione limacina. VII Reexamination of type 12 interneurons.* Exp Brain 1986. **63**: p. 106–112.
6. Arshavsky Y. I., Orlovsky G. N., Panchin Y. V., Roberts A., Soffe S. R. , *Neuronal control of swimming locomotion: analysis of the pteropod mollusc Clione and embryos of the amphibian Xenopus* Trends Neurosci, 1993. **16**: p. 227–233.
7. Arshavsky Y. I., *Cellular and network properties in the functioning of the nervous system: from central pattern generators to cognition.* Brain Research Reviews, 2002. **41**(2-3): p. 229-267.
8. Bedrov Y. A., Dick O. E. ,Nozdrachev A. D., Akoev G. N., *Method for constructing the boundary of the bursting oscillations region in the neuron model.* Biol. Cybern., 1999. **82**: p. 493-497.

9. Belykh V.N. , Belykh I.V. , Colding-Jørgensen M.,Mosekilde E. , *Homoclinic bifurcations leading to the emergence of bursting oscillations in cell models.* Eur. Phys. J. E 2000. **3**: p. 205–219.

10. Breakspear, M., ,Roberts, J. A., Terry J. R, Rodrigues S., Mahant N., Robinson P. A, *A Unifying Explanation of Primary Generalized Seizures Through Nonlinear Brain Modeling and Bifurcation Analysis.* Cereb. Cortex , 2006. **16**(9): p. 1296-1313.

11. Calabrese RL, N.F., Olsen OH., *Heartbeat control in the medicinal leech: a model system for understanding the origin, coordination, and modulation of rhythmic motor patterns.* J Neurobiol., 1995. **27(3):**: p. 390-402.

12. Cohen A. H., Rossignol S., and Grillner S., *Neuronal Control of rhythmic movements in vertebrates.* eds New York: Wiley., 1988: p 865-872.

13. Cymbalyuk G. S., Calabrese R. L., *Oscillatory behaviors in pharmacologically isolated heart interneurons from the medicinal leech.* Neurocomputing, 2000. **32-33**: p. 97-104.

14. Cymbalyuk G. S. and Calabrese R. L., *A model of slow plateau-like oscillations based upon the fast Na current in a window mode.* Neurocomputing 2001. **38-40**: p. 159-166.

15. Cymbalyuk Gennady S., Gaudry Q., Masino M. A., Calabrese R. L., *Bursting in Leech Heart Interneurons: Cell-Autonomous and Network-Based Mechanisms.* J. Neurosci., 2002. **22**(24): p. 10580-10592.

16 Cymbalyuk G.S., Shilnikov A.L., Calabrese R.L. *Yin and Yang of Leech Heart Central Pattern Generator: Endogenously Bursting Neurons Yoked Together into a Half-Center Oscillator.* Society for Neuroscience conference 2003.

17. Darbon P., Cedric Y., Legrand J., Streit J., *INaP underlies intrinsic spiking and rhythm generation in networks of cultured rat spinal cord neurons.* European Journal of Neuroscience, 2004. **20**: p. 976-988.

18. DeLorenzo R. J., Sun D. A., and Deshpande Laxmikant S., *Cellular mechanisms underlying acquired epilepsy: The calcium hypothesis of the induction and maintainance of epilepsy*, in *Pharmacology & Therapeutics*. 2005. p. 229-266.

19. Drongelen W., Koch H., Marcuccilli C., Hecox K., Ramires M., *Is burst activity in cortical slices a representative model for epilepsy?* Neurocomputing, 2003. **52-54**: p. 963-968.

20. Edwards D. H., Heitler, Krasne W. J., Franklin B., *Fifty years of a command neuron: the neurobiology of escape behavior in the crayfish.* Trends in Neurosciences, 1999. **22**(4): p. 153-161.

21. Francis, J.T., Gluckman B.J., and S.J. Schiff, *Sensitivity of Neurons to Weak Electric Fields.* J. Neurosci., 2003. **23**(19): p. 7255-7261.

22. Feudel U. and Grebogi C., *Multistability and the control of complexity.* Chaos, 1997. **7(4)**: p. 597-605.

23 Friesen, W.O. and G.S. Stent, *Neural Circuits for Generating Rhythmic Movements*. 1978. p. 37-61.

24. Fröhlich F., Bazhenov M., *Coexistence of tonic firing and bursting in cortical neurons.* Phys. Rev, 2006. **74**.

25. Gadaleta S., Dangelmayr G., *Learning to control a complex multistable system.* PhysRevE, 2001. **63**: p. 1-12.

26. Guckenheimer J. and Tien J. H. , *Bifurcation in the fast dynamics of neurons: implication for bursting.* 2003: p. 89-122.

27. Harvey A. S. and Freeman J. L., *Epilepsy in Hypothalamic Hamartoma: Clinical and EEG Features.* Hypothalamic Hamartoma, 2007. **14**(2): p. 60-64.

28. Hill A. A., Lu J., Masino M. A., Olsen O. H., Calabrese R. L., *A Model of a Segmental Oscillator in the Leech Heartbeat Neuronal Network.* Journal of Computational Neuroscience, 2001. **10**(3): p. 281-302.

29. Huxley, A. F., *Hodgkin and the action potential 1935-1952.* J Physiol, 2001.014118, 2002. **538**(1): p. 2-.

30. Izhikevich E. M., *Neural Excitability, Spiking And Bursting.* International Journal of Bifurcation and Chaos, 1999. **10**: p. 1171-1266.

31. Katz, P.S., et al., *Cycle Period of a Network Oscillator Is Independent of Membrane Potential and Spiking Activity in Individual Central Pattern Generator Neurons*. 2004. p. 1904-1917.

32. Kristan Jr. W. B., Calabrese R. L., and Friesen W. O., *Neuronal control of leech behavior.* Progress in Neurobiology, 2005. **76**(5): p. 279-327.

33. Lafreniere-Roula, M. and D.A. McCrea, *Deletions of Rhythmic Motoneuron Activity During Fictive Locomotion and Scratch Provide Clues to the Organization of the Mammalian Central Pattern Generator*. 2005. p. 1120-1132.

34. Levitan I. B. and Kaczmarek L. K., *The Neuron cell and molecular biology*. second edition. 1997: Oxford University Press.

35. Li, W.C., S.R. Soffe, and A. Roberts, *Dorsal Spinal Interneurons Forming a Primitive, Cutaneous Sensory Pathway*. 2004. p. 895-904.

36. Lu J., Dalton J., Stokes D. R., Calabrese Ronald L., *Functional Role of Ca2+ Currents in Graded and Spike-Mediated Synaptic Transmission Between Leech Heart Interneurons.* J Neurophysiol, 1997. **77**(4): p. 1779-1794.

37. Manning J.A., Richards D., and Bowery N., *Pharmacology of absence epilepsy.* Trends in Pharmacological Science, 2003. **24**.

38. Manuca R. , Casdagli M. C. , Savit R. S., *Nonstationarity in Epileptic EEG and Implications for Neural Dynamics.* Math Bioscience, 1998. **147**: p. 1-22.

39. Marder E. and Calabrese R.L., *Principles of rhythmic motor pattern generation*. Physiol Rev., 1996. p. 687-717.

40. Masino M. A. and Calabrese R. L., *A Functional Asymmetry in the Leech Heartbeat Timing Network Is Revealed by Driving the Network across Various Cycle Periods.* J. Neurosci., 2002. **22**(11): p. 4418-4427.

41. Milton J. and Jung P., *Epilepsy as a Dynamical Disease*. 2003, New York: Springer-Verlag Berlin Heidelberg. 411.

42. Nadim, F. and Calabrese R.L., *A Slow Outward Current Activated by FMRFamide in Heart Interneurons of the Medicinal Leech.* J. Neurosci., 1997. **17**(11): p. 4461-4472.

43. Netoff T. I., Schiff S. J., *Decreased Neuronal Synchronization during Experimental Seizures*. J. Neurosci., 2002. p. 7297-7307.

44. Olsen O. H. and Calabrese R. L., *Activation of intrinsic and synaptic currents in leech heart interneurons by realistic waveforms.* J Neurosci, 1996. **16:**: p. 4958–4970.

45. Olsen O. H., Nadim F., and Calabrese R. L., *Modeling the leech heartbeat elemental oscillator. II. Exploring the parameter space.* J Comput Neurosci 1995. **2:**: p. 237–257.

46. Olypher, A., Cymbalyuk G. S., and Calabrese R.L., *Hybrid Systems Analysis of the Control of Burst Duration by Low-Voltage-Activated Calcium Current in Leech Heart Interneurons*. J. Neorophysiol., 2006. p. 2857-2867.

47. Perlmutter J. S. and Mink J. W., *Deep Brain Stimulation.* Annu. Rev. Neurosci., 2006. **29**: p. 229-257.

48 Ramirez, J.-M. and J.-C. Viemari, *Determinants of inspiratory activity.* Respiratory Physiology & Neurobiology, 2005. **147**(2-3): p. 145-157.

49 Rinzel J. (1985) Bursting oscillations in an excitable membrane model. In: Sleeman BD, Jarvis RJ, eds. Ordinary and partial Differential Equations. Proceedings of the 8th Dundee Conference. Lecture Notes in Mathematics, 1151. Berlin: Springer, 304-316.

50. Shilnikov A., Calabrese R., and Cymbalyuk S. G., *Mechanism of bi-stability: tonic spiking and bursting in a neuron model.* Comp. Neurosci., 2004.

51. Shilnikov L. P. and Shilnikov A. L., *Methods of qualitative theory in nonlinear dynamics* Vol. 1. 2001. 389.

52. Shilnikov L. P. and Shilnikov A. L., *Methods of qualitative theory in nonlinear dynamics* Vol. 2. 2001.

53. Simon T.W., Schmidt J., and Calabrese R.L., *Modulation of high-threshold transmission between heart interneurons of the medicinal leech by FMRF-NH2.* J Neurophysiol, 1994. **71**(2): p. 454-466.

54. Solis, M.M. and D.J. Perkel, *Rhythmic Activity in a Forebrain Vocal Control Nucleus In Vitro*. 2005. p. 2811-2822.

55. Steriade M., Grenier F., *Natural Waking and Sleep States: A View From Inside Neocortical Neurons*. J. Neurophysiol., 2001. p. 1969-1985.

56. Strogatz S. H., *Nonlinear dynamics and chaos, 1998*

57. Tass P. A., *Desynchronizing double-pulse phase resetting and application to deep brain stimulation.* Biol. Cybern., 2001. **85**: p. 343-354.

58. Tass P. A., Hauptmann C., *Therapeutic modulation of synaptic connectivity with desynchronizing brain stimulation.* International Journal of Psychophysiology, 2007. **64**(1): p. 53-61.

59 Tryba, A.K., F. Pena, and J.-M. Ramirez, *Gasping Activity In Vitro: A Rhythm Dependent on 5-HT2A Receptors*. 2006. p. 2623-2634.

60. Wang X., Golomb D., and Rinzel J., *Emergent Spindle Oscillations and Intermittent Burst Firing in a Thalamic Model: Specific Neuronal Mechanisms.* PNAS, 1995. **92**(12): p. 5577-5581.

61. Weese-Mayer D., Ackerman M. J., Marazita M. L., Berry-Kravis E. M., *Sudden Infant Death Syndrome: Review of implicated genetic factors.* American Journal of Medical Genetics Part A, 2007. **143A**(8): p. 771-788.

62. Yakovenko, S., McCrea D.A., Stecina K. Prochazka A., *Control of Locomotor Cycle Durations*. J. Neurophysiol., 2005. p. 1057-1065.

63 Somjen G.G., *Ions in the Brain: Normal Function, Seizures, and Stroke.* Oxford University Press, NewYork, 2004.

64 Jensen M. S. and Yaari Y., *Role of Intrinsic Burst Firing, Potassium Accumulation, and Electrical Coupling in the Elevated Potassium Model of Hippocampal Epilepsy*. J. Neurophysiol. 77, 1224 1997 ;